The Journal of Adhesion

ISSN: 0021-8464 (Print) 1545-5823 (Online) Journal homepage: www.tandfonline.com/journals/gadh20

Life prediction of adhesive steel joints under ageing stress – experimentally based model validation

Jannis Damm, Thomas Ummenhofer , Matthias Albiez, Gerson Meschut , Sascha Sander , Dominik Teutenberg & Fabian Kötz

To cite this article: Jannis Damm, Thomas Ummenhofer , Matthias Albiez, Gerson Meschut , Sascha Sander , Dominik Teutenberg & Fabian Kötz (19 May 2026): Life prediction of adhesive steel joints under ageing stress – experimentally based model validation, The Journal of Adhesion, DOI: 10.1080/00218464.2026.2671924

To link to this article: https://doi.org/10.1080/00218464.2026.2671924

Published online: 19 May 2026.

THE JOURNAL OF ADHESION
https://doi.org/10.1080/00218464.2026.2671924

Life prediction of adhesive steel joints under ageing stress – experimentally based model validation

Jannis Damm[a], Thomas Ummenhofer[a], Matthias Albiez[a], Gerson Meschut[b], Sascha Sander[b], Dominik Teutenberg[b], and Fabian Kötz[c]

[a]Karlsruhe Institute for Technology (KIT), Steel- and Lightweight Structures, Karlsruhe, Germany; [b]Laboratory of Materials and Joining Technology, Paderborn University, Paderborn, Germany; [c]Institute for Mechanics, Kassel University, Kassel, Germany

ABSTRACT

Predicting the ageing behaviour of adhesively bonded joints is a key challenge in adhesive bonding technology and is essential for their broader use in steel construction. This paper presents a method for predicting the long-term performance of thick-layer adhesive bonds under hygro-thermo-mechanical (htm) stress. This approach is based on experimental investigations into the water absorption of the adhesive, which is recorded gravimetrically and described using Fickian´s diffusion model. Different temperature and humidity influences on the diffusion parameters are considered using an Arrhenius approach. The mechanical behaviour is analysed by means of quasi-static tests and systematic creep experiments different specimen geometries. Numerical modelling is based on an adhesive layer equivalent model that represents the linear viscoelastic behaviour and damage resulting from htm loading. Temperature and humidity influences are recorded via a time-temperature-water concentration shift, and the multi-axial nature of the failure is described via a comparative stress. Validation is performed using component-like specimens and transient FE simulations with LS-DYNA, which utilise the coupling of diffusion and heat conduction problems. The case study shows that the developed concept enables a reliable life prediction and thus contributes significantly to confidence in adhesive bonding technology.

ARTICLE HISTORY
Received 16 January 2026
Accepted 5 May 2026

KEYWORDS
Adhesive bonding; ageing; Fickian´s diffusion; long-term behaviour; hygro-thermo-mechanical loading; lifetime prediction; viscoelasticity

1. Introduction

1.1. Fields of application for adhesive bonding technology in steel construction

Load-bearing adhesive bonds have been successfully applied in automotive and aerospace engineering for decades.[1–3] Owing to their numerous advantages, components such as body panels, windscreens, and panoramic roofs are increasingly joined using adhesive technologies.[4] In the growing field of electromobility, adhesives are also essential for assembling batteries and

CONTACT Jannis Damm jannis.damm@kit.edu Karlsruhe Institute for Technology (KIT), Steel- and Lightweight Structures, Karlsruhe, Germany

sensors.[5] Compared to conventional joining methods, adhesive bonding offers significant benefits, including reduced weight, lower costs, and enhanced crash safety.

In the construction industry, the use of adhesives and structural adhesive bonds is limited to individual applications. A broad field of application for adhesives in the construction industry is sandwich elements for finishes and thermal insulation. Structural glazing enables the linear bonding of large glass panes to metal or timber support frames without introducing stress concentrations.[6] In the field of steel construction, a large number of research papers have been published in recent years on the analytical stress calculation of bonded joints with flat and cylindrical bonded layers and the associated static load-bearing capacity[7–11] as well as on the dynamic properties of bonded joints.[12–17] The work mentioned above contributes to the development of new fields of application through research projects on the use of structural adhesive bonds in the offshore sector.[18,19] Subsequent work investigates the practical use of viscoelastic adhesive properties for damping dynamically loaded structures.[20–22]

Furthermore, research into new joining concepts is being conducted.[23–25] The hybrid adhesive-grout connection technology, which is particularly suitable for joining hollow section tubular joints, has a novel, multi-layered structure. Here, inorganic and organic adhesive layers are combined, whereby a very high mechanical load-bearing capacity of the joint is achieved.[23] The hybrid bolted connections presented in[24] combine pretensioned bolts and adhesive joints. This allows the static load-bearing capacity to be significantly increased by using the hybrid screw connection compared to conventional screw connections.

In addition to the use of structural bonding as load-bearing connections, the use of bonded CFRP laminates for refurbishment of buildings is investigated. In,[26,27] the possibility of retrofitting fatigue-damaged steel structures with slack and prestressed CFRP laminates is investigated. A significant increase in the remaining service life compared to an unreinforced beam can be determined.

For all of the above-mentioned applications, adhesive bonds are subject to planned ageing effects from temperature, humidity and long-term mechanical stress, which must be assessed in advance by calculation.

1.2. Long-term load-bearing behaviour of adhesively bonded joints under ageing exposure

The ageing of polymers and adhesives subjected to continuous stress due to prolonged exposure or service life is a complex process involving physical and chemical changes. Adhesives are subject to these ageing mechanisms, which influence the material properties and reduce the service life of the joints.[28]

Physical ageing occurs when a material strives for a state of thermodynamic equilibrium without external influences such as mechanical stress or environmental conditions.[29,30] It leads to an increase in density, volume shrinkage and changes in the viscoelastic properties. This process is thermo-reversible[31] and does not lead to permanent degradation or failure of the material.

In contrast, chemical ageing describes irreversible material changes as a result of chemical reactions triggered by external factors such as moisture or temperature.[28] A central mechanism is moisture diffusion, in which water molecules penetrate the adhesive layer, cause volume and mass changes and can cause competitive adsorption between the steel surface and the adhesive molecules.[32–36]

The effects of moisture diffusion are both reversible and irreversible. Reversible changes, such as in the glass transition area, can be eliminated by re-drying. Irreversible damage, however, such as hydrolysis of the polymer chains, remains and leads to a permanent loss of mechanical load-bearing capacity. Mechanical stresses play a significant role in accelerating chemical ageing, as they reduce the activation energy for hydrolytic processes.[37] This promotes the decomposition of polymer chains and further deteriorates the mechanical properties of the adhesive bond. The diffusion of moisture into the adhesive layer is a critical factor that significantly influences the mechanical properties.[32,38–43] Moisture absorption can not only reduce strength, but also cause corrosion and detachment of the adhesive layer from the substrate. Experiments under controlled climatic conditions show a strong dependence of chemical ageing on temperature and humidity. The static strength and long-term behaviour of the adhesive bonds are significantly influenced by these factors.[44] Han et al.[45] investigates the residual static strength of adhesively bonded joints after long-term exposure to a combined mechanical – hygro – thermal environment. The degradation process is modeled using a fully coupled approach in which moisture diffusion and stress distribution interact. Progressive failure of the aged joints is simulated using a bilinear cohesive zone model in a finite element framework, incorporating degradation due to creep strain and moisture uptake. The numerical predictions show good agreement with experimental results.

Studies also show that the combined effects of temperature, moisture and mechanical stress can significantly accelerate ageing.[46] Thermal and hygro influences in particular significantly reduce the strength of bonded steel joints.[42,43,47–49] In investigations on test specimens with inhomogeneous mechanical, thermal and hygro stress (htm stress), it was found that the influences of the process parameters often occur superimposed, which makes a differentiated analysis more difficult.[32,38–41,48–50] To circumvent this, experiments were carried out in[46] in which homogeneous load fields were created in the adhesive layer. This method enables a targeted investigation of the individual parameters. The use of specific surface treatments, such

as phosphate or oxide coatings, has been shown to reduce the corrosion of steel components induced by hydrolysis.[46,51] These protective layers prevent corrosion at the interface and help to preserve the mechanical properties, which significantly improves the durability of adhesive bonds. In the work by Han et al.[52] a numerical modelling techniques to simulate the combined effects of moisture, elevated temperature, and mechanical loading on adhesively bonded joints is developed. A fully coupled approach is used, where moisture diffusion and stress distribution interact, while moisture-dependent creep, swelling, and thermal strains are included in the stress analysis. Model parameters are derived from experiments on the bulk adhesive, and the predicted joint response during ageing shows good agreement with experimental results.

1.3. Modelling and simulation of adhesive joint failure under ageing effects

Although there are numerous standards and guidelines for testing bonded joints under the influence of ageing, ageing has so far been insufficiently considered in the mathematical design. This leads to high safety factors for bonded components, such as in EAD 090010–00–0404.[53]

In[46], a new concept was presented that recognises the failure mechanism due to ageing influences and implements it mathematically. The concept is based on a transient finite element calculation that simulates the long-term and failure behaviour of structural epoxy adhesive joints. It includes the characterisation of the diffusion and mechanical long-term behaviour. The diffusion characterisation is carried out gravimetrically and is implemented in the finite element simulation as Fickian´s diffusion. The mechanical behaviour is described with a rheological model, which depicts additional reversible and irreversible damage mechanisms within the cohesive zone elements.

The model combines the principle of effective stress with a damage model whose parameters are identified from creep fracture tests under thermo-mechanical loads. The viscoelastic properties of the adhesive are taken into account at arbitrary temperatures using the time-temperature-water concentration shift principle from dynamic mechanical temperature analysis (DMTA) data. The model is implemented as a user-defined material in LS-DYNA and enables the simulation of damage and failure up to complete material fracture. With this approach, the long-term failure of structural adhesive joints under hygro-thermo-mechanical loads was predicted with high accuracy. However, the model is not applicable to thick, semi-structural PU adhesive layers due to the differentiated mechanical material behaviour. As the model is fundamentally designed for a cohesive zone, and thus for thin adhesive layers, i.e. structural adhesives, it cannot be directly applied to thick adhesive layers. One can approximate this by using the cohesive zone multiple times and inserting viscoelastic zones between them for the FE modelling (see

image: FE model), or by reformulating the model using SOLID elements and meshing with multiple elements across the adhesive layer thickness. Only by using multiple elements across the adhesive layer thickness can the necking and the correct deformation pattern be reproduced and taken into account. Additionally, the model was extended to include hygro influences and implemented using model adjustments and identified parameters from the dynamic mechanical temperature (water) concentration analysis DMTCA.

A fracture mechanics approach was developed in[54] for transfer to semi-structural adhesive joints. Here, the adhesive layer is meshed with several elements across the thickness, whereby hyperelastic material behaviour is considered. Cohesive zone elements model the adhesive layer failure. Simulations show that the approach describes the force-displacement behaviour of semi-structural PU adhesives well. However, the viscoelastic creep deformations cannot be captured by purely hyperelastic models.

In,[55–59] a hyperelasticity model was therefore supplemented by a viscoelastic spectrum, which is identified using dynamic mechanical analysis (DMA). DMA utilises the principle of time-temperature shift to determine relaxation times and modulus components that represent viscoelastic phenomena over a large period of time.[60]

1.4. Scope of this paper

The current work is based on the results published in.[61] In,[61] the results of fundamental work on identifying the parameters necessary for developing a diffusion and substitute model of the adhesive to take into account combined hygro-thermo-mechanical (htm) stress on the short- and long-term behaviour of adhesive bonds are presented.

Building on this, the scope of this paper is set on two aspects. Firstly, the results of experimental short-term and long-term tensile tests on adhesively bonded specimens under ageing stress are presented. The focus is on identifying the influence of ageing effects due to temperature and humidity in combination with mechanical stress on the short-term and especially the long-term load-bearing behaviour of adhesively bonded joints on a large scale. The selection of test specimens with thick-film adhesives, which are already used in automotive and aircraft construction or could be used in glass façade construction (structural glazing),[62] addresses an existing gap in the state of research.

In addition to the experimental investigations, an analytical adhesive layer substitute model is being developed, consisting of a rheological model and a damage model. The approach is based on the work described in[46] and on data from experimental and analytical studies on standardised small test specimens published in.[61] The model formulations contained in[61] are adapted and optimised for use in thick-film bonding of steel substrates.

The conclusion is a validation of the developed adhesive layer replacement model based on the aforementioned experimental data from long-term tests on component-like H-specimens. In this regard, it is being investigated whether semi-structural polyurethane adhesives have the necessary hygro-rheological simplicity to be able to apply a time-water concentration shift. Furthermore, it is being analysed whether a DMA-based spectrum can be transferred to semi-structural bonds with large deformations.

2. Materials and methods

2.1. Materials and specimens

2.1.1. Adhesives

A total of three adhesive systems were investigated within this study. The results of the adhesive characterisation are comprehensively documented in.[61,63] Based on the findings of the adhesive characterisation studies, the 2-component polyurethan adhesive BETAFORCE 2817 V1 of DuPont Specialty Products GmbH & Co. KG® is selected for the further examinations and referred to as adhesive BETAFORCE. The adhesive is used in combination with the 2-component adhesion promoter BETAPRIME 1707 of DuPont Specialty Products GmbH & Co. KG®.

2.1.2. Steel materials: T-profile sections

The modified H-specimen used in the investigations consists of two isosceles T-profile (steel grade S355) sections of T50×50×5 with a length of 100 mm. The specimens are bonded with an adhesive layer thickness of 6 mm and an adhesive layer width of 12 mm. The adhesive layer runs along the entire length of the T-profile sections. The dimensions shown in Figure 1 are nominal values.

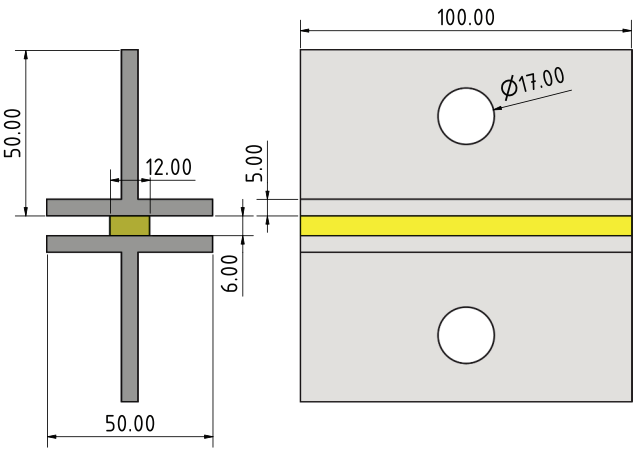

Figure 1. Schematic representation of the modified H-specimen.

2.2. Numerical modelling

2.2.1. Preliminary remark

This section describes the development of a model for calculating the long-term load-bearing behaviour of bonded joints under ageing stress. The behaviour of the adhesive layer is described using a rheological model that takes damage into account. The influences of the ageing effects of temperature and humidity on the load-dependent load-bearing behaviour are taken into account.

Basic adhesive characterisation tests and the associated results are documented in.[61] The necessary material parameters identified from these tests for the development of the material model are also documented in.[61] This section focuses on the creation and validation of the model equations.

2.2.2. Ageing time of the test specimens

To characterise the influence of moisture on the short and long-term behaviour of the test specimens, a defined moisture content of the adhesive layer must be generated at the start of the test. This can be achieved by ageing the test specimens under defined temperature and humidity boundary conditions. The duration of the ageing of the test specimens to achieve a defined moisture concentration can be determined using Fickian´s second equation with Equation 1.[64]

$$\frac{M_t}{M_\infty} = 1 - \frac{8}{\pi^2} \sum_{i=0}^{\infty} \frac{\exp\left(\frac{-D(2i+1)^2\pi^2 t}{d_k^2}\right)}{(2i+1)} \tag{1}$$

In Equation 1, M_t and M_∞ are the water masses at time t and at saturation, respectively, D is the diffusion coefficient independent of location and concentration, and d_k is the thickness of the adhesive layer. The water mass at saturation M_∞ follows from Equation 2

$$M_\infty = A \times d_k \times c_\infty = V \times c_\infty \tag{2}$$

The determination and verification of the temperature-dependent diffusion coefficients required for calculating the release times were described in other publications by the authors.[61,63] The focus of this paper is on the practical application of the formulas presented.

The adhesive layers in the joints must be able to be soaked with water within an appropriate period of time so that the adhesive joint has a defined water concentration and the influence of moisture on the ageing behaviour can be specifically investigated.

In all subsequent mechanical investigations, the adhesive layer is in a fully saturated condition. To ensure a homogeneous moisture distribution throughout the entire adhesive thickness, all specimens were conditioned until at least

99% saturation was reached at every point of the adhesive layer. The required conditioning times were derived from gravimetric diffusion measurements on bulk adhesive samples and numerical evaluations of the diffusion equation. This procedure guarantees identical moisture levels in core and edge regions and eliminates any specimen-size dependency during mechanical testing. By imposing a fully saturated and spatially uniform initial moisture field, no diffusion processes occur during mechanical loading, and thus no interaction between stress-assisted diffusion and creep-related transport can arise within the experiments conducted in this study.

For the calculation of the duration of the diffusion processes, the steel joining parts are assumed to be diffusion barriers for the sake of simplicity. In addition, a completely dry adhesive layer is assumed at the start of the diffusion process, so that the initial concentration c_t is zero in the whole adhesive layer.

2.2.3. General constitutive equation and concept of effective stress

For reasons of numerical efficiency, the adhesive layer is considered to be the interface between the steel substrates. The creep deformations of this adhesive layer that occur as a result of the applied constant mechanical stress can be divided into primary, secondary and tertiary components. Primary and secondary creep mainly result from the viscoelasticity of the adhesive, which can be reversibly restored by moistening and re-drying. In contrast, tertiary creep is mainly caused by damage due to irreversible breaking of molecular bonds through combined mechanical stress and hydrolysis. The adhesive layer model for describing the complete creep behaviour, which is created as a cohesive zone model, consists of a part for describing the effective, damage-free material behaviour (primary and secondary creep) and a part for taking irreversible damage into account (tertiary creep).

The effective behaviour in the form of the relationship between the displacement jump Δ and the effective Cauchy stress $\tilde{\sigma}$ is described according to Equation 3 in the one-dimensional case without physical ageing by the following functional F:

$$\tilde{\sigma}(t) = F_{s=0}^{s=\infty}(\Delta(t-s)) \tag{3}$$

The constitutive equation (Equation 3) is applied together with the concept of effective stress according to [65] and,[66] via which the damage D_{ca} is introduced and the physical Cauchy stress σ is calculated:

$$\sigma = (1 - D_{ca})\tilde{\sigma}, D_{ca} \in [0, 1] \tag{4}$$

The damage variable D_{ca} assumes values from zero to one according to Equation 3. $D_{ca} = 0$ indicates undamaged material and $D_{ca} = 1$ indicates complete material separation. The development of damage over time as a result of

mechanical, hygro and thermal stress is described by an ordinary differential equation of the first order – the damage differential equation:

$$\dot{D}_{ca} = \dot{D}_{ca}(D_{ca}, \sigma, c, T) \tag{5}$$

2.2.4. Damage model

The damage differential equation (Equation 5) must be specified in order to be able to map the long-term failure due to mechanical, hygro and thermal stress. It is assumed here that the total damage development D_{ca} is composed of a creep D_c and ageing component $\dot{D}_{ca}$ additive according to[67]:

$$\dot{D}_{ca}(\sigma, c, T) = \dot{D}_c(\sigma, T) +_a(\sigma, T) \tag{6}$$

The expression $\dot{D}_c(\sigma, T)$ describes the temperature-dependent creep damage and the expression $\dot{D}_a(\sigma, T)$ describes the temperature-dependent ageing damage. For the creep damage development $\dot{D}_c$, the approach of[65] according to Equation 7 is used in the isothermal case.

$$\dot{D}_c = \frac{1}{c_0}\left(\frac{\sigma}{\sigma_{ref}(1 - D_{ca})}\right)^n, c_0 = 1s \tag{7}$$

In doing so, c_0 establishes consistency between the units, and the parameter σ_{ref} to be identified scales the past damage. For the hygro-damage development $\dot{D}_a$ in Equation 6 the following approach is used for the damage development due to oxidation based on,[68] where $l = 1$:

$$\dot{D}_a = B_A(1 - D_{ca})\left(\frac{c}{c_{\infty,ref}}\right)^l \exp\left(p_a\left(\frac{1}{T_{refa}} - \frac{1}{T}\right)\right) \tag{8}$$

B_A, l and $c_{\infty,ref}$ are parameters to be identified for isothermal hygrodamage. The influence of temperature is considered by identifying the parameter p_a. Like T_{refc} in the creep damage approach Equation 9, the reference temperature T_{refa} is set to $T_{refa} = T$ for the isothermal case and is otherwise defined in the order of magnitude of the operating temperature of the adhesive layer. The damage differential equation Equation 6 with the approaches according to Equation 7 and Equation 8 is as follows[69]:

$$\begin{aligned}\dot{D}_{ca}(\sigma, c, T) = &\frac{1}{c_0}\left(\frac{\sigma}{\sigma_{ref}(1 - D_{ca})}\right)^n \exp\left(p_c\left(\frac{1}{T_{refc}} - \frac{1}{T}\right)\right) \\ &+ B_A(1 - D_{ca})\left(\frac{c}{c_{\infty,ref}}\right)^l \exp\left(p_a\left(\frac{1}{T_{refa}} - \frac{1}{T}\right)\right)\end{aligned} \tag{9}$$

Finally, the multiaxiality is considered in the damage model by defining the equivalent stress σ_{eqc}, so that the following expression is used instead of the creep damage development Equation 7:

$$\dot{D}_c = \frac{1}{c_0}\left(\frac{\sigma_{eqc}}{\sigma_{ref}(1-D_{ca})}\right)^n \exp\left(p_c\left(\frac{1}{T_{refc}}-\frac{1}{T}\right)\right) \tag{10}$$

The approach from,[70] which has already proven its worth in describing the influence of the stress multi-axiality on the creep damage for the structural adhesive investigated in this project, is used for the comparative stress σ_{eqc} occurring here:

$$\sigma_{eqc} = \sqrt{\langle b_{1c}t_n{}^2 + b_{2c}t_n + t_t^2 + t_b{}^2\rangle} \tag{11}$$

t is a stress vector for normal, tangential and binormal stresses. The components of the damage model developed are summarised in Table 1 together with the parameters to be identified.

2.2.5. Rheological model

The rheological model for describing the linear viscoelasticity in the area of primary and secondary creep is created on the basis of Equation 3. In the course of this, the functional F must be defined in the general constitutive equation (Equation 3). In the Wiechert model, the relaxation time

$$\hat{\tau}_i = \eta_i/k_i \tag{12}$$

of chain i, which depends on the viscosity η_i and stiffness k_i of chain i. The number of Maxwell chains is $\bar{M}$.

Figure 2 shows the Wiechert model on the left. It describes the general visco-elastic flow behaviour and is associated with the elementary spring and damper elements of the model rheology. If the relaxation time of the Maxwell chain $\bar{M}$ is infinitely large, this can be taken into account by eliminating the damper arranged in series with it, see Figure 2 (right) with $M = \bar{M}-1$. The remaining stiffness $k_{\bar{M}}=k_\infty$ is referred to as the equilibrium stiffness, to which the displacement jump Δ_∞ is assigned. Due to the introduction of the equilibrium chain with stiffness k_∞ just described, it can be concluded that the following applies[71,72]:

Table 1. Summary of the damage model with parameters to identify [63].

Designation	Equation	Parameters
Total damage	$\dot{D}_{ca} = \dot{D}_c + \dot{D}_a$	
Creep damage	$\dot{D}_c = \frac{1}{c_0}\left(\frac{\sigma_{eqc}}{\sigma_{ref}(1-D_{ca})}\right)^n \exp\left(p_c\left(\frac{1}{T_{refc}}-\frac{1}{T}\right)\right)$	n, σ_{ref}, p_c
Equivalent tension	$\sigma_{eqc} = \sqrt{b_{1c}t_n{}^2 + b_{2c}t_n + t_t^2 + t_b}$	b_{1c}, b_{2c}
Hygro damage	$\dot{D}_a = B_A(1-D_{ca})\left(\frac{c}{c_{\infty,ref}}\right)^l \exp\left(p_a\left(\frac{1}{T_{refa}}-\frac{1}{T}\right)\right)$	l, B_a, p_a
Concept of effective tension	$t = [t_t \quad t_b \quad t_n]^T = (1-D_{ca})\tilde{t}$	

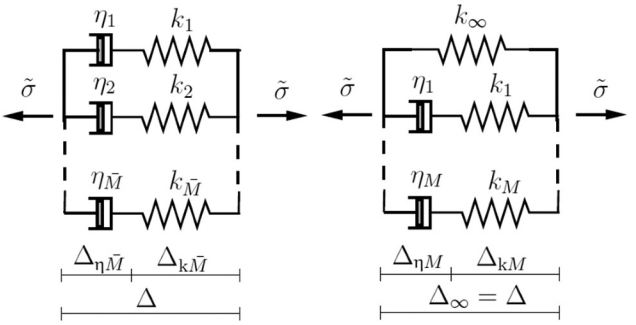

Figure 2. Wiechert model (left) and generalised Maxwell model with equilibrium chain (right).

$$R(t-\tau) = k_\infty + \sum_{i=1}^{M} k_i \exp(-(t-\tau)/\hat{\tau}_i) \tag{13}$$

Substituting Equation 13 into the constitutive results in:

$$\hat{\sigma}(t) = \int_0^t k_\infty + \sum_{i=1}^{M} k_i \exp(-(t-\tau)/\hat{\tau}_i) \frac{d\Delta(\tau)}{d\tau} d\tau = \hat{\sigma}_\infty(t) + \hat{\sigma}_{OV}(t) \tag{14}$$

The expressions $\hat{\sigma}_\infty$ and $\hat{\sigma}_{OV}$ are called effective equilibrium stress and effective overstress respectively.

2.2.5.1. Influence of temperature on the viscoelastic properties. The influence of temperature on the viscoelastic properties of polymers is often determined using the time-temperature-shift principle (TTS).[74,75] A material to which the TTS can be applied is referred to as a thermorheologically simple material. This structural adhesive is a thermosetting epoxy resin that is filled with rubber particles and forms a filled duromer when cured. Since both individual components are polymers, it is appropriate to assume thermorheological simplicity when modelling the influence of temperature on the viscoelastic material behaviour, as in the works [76,77].

The relaxation function R(t,T) at time t and a fixed temperature T is related to the relaxation function $R_{T0}(\xi)$ at the reference time/reduced time/material time ξ and reference temperature T_0 as follows[74,78]:

$$R(t,T) = R_{T0}(\xi); \xi = \frac{t}{\alpha_T} \Rightarrow R(t,T) = R_{T0}\left(\frac{t}{\alpha_T}\right) \tag{15}$$

The variable $\alpha_T = \alpha_T(T)$ is the time-temperature shift function, also known as the "shift factor". It indicates how far the relaxation function is shifted horizontally at a certain temperature T compared to the reference temperature T_0 on a logarithmic scale. The horizontal shift is present for both the relaxation

function and the creep function. In the general non-isothermal case, the following expression is used instead of Equation 15[73,78,79]:

$$\xi = \xi(t) = \int_0^t \frac{1}{\alpha_T(T(\tilde{\tau}))}, \qquad dt = \alpha_T d\xi \tag{16}$$

The reduced time in Eq. 16 corresponds to the isothermal case $T(\tilde{\tau}) = T = cost \rightarrow \alpha_T = \alpha_T(T(\tilde{\tau})) = \alpha_T(T)$ after evaluation of the integral in Equation 15 The presented modelling of the influence of temperature has a reversible character in the chemical sense: A material has certain viscoelastic properties at a certain homogeneous initial temperature. When the temperature is changed, the viscoelastic properties change. However, if the material returns to the initial temperature, the original viscoelastic properties are also restored.

2.2.5.2. Influence of moisture on the viscoelastic properties. The influence of moisture on the viscoelastic properties is recorded in [80,81] analogue to the influence of temperature. This means for Equation 15:

$$R(t, c) = R_{c0}(\xi), \xi = t/\alpha_c \Rightarrow R(t, c) = R_{c0}(t/\alpha_c) \tag{17}$$

The function $\alpha_c = \alpha_c(c)$ is the time-concentration-shift function. In the general case of a non-constant concentration, the reduced time and history are defined analogously to Eq. 16 as follows[69]:

$$\xi = \xi(t) = \int_0^t \frac{1}{\alpha_c(c(\tilde{\tau}))} d\tilde{\tau}, \qquad \tilde{\xi} = \xi(t) \tag{18}$$

The influence of moisture on the viscoelastic properties has the same reversible character in the chemical sense as the influence of temperature: A material with a certain moisture content or with a certain homogeneous initial concentration has certain viscoelastic properties. These can be restored if the material is dried or moistened back to this initial concentration. According to the analogy of Eq. 17 and Eq. 18 with Equation 15 and Eq. 16 for thermorheological simplicity, the concept just presented is referred to as hygrorheological simplicity.

2.2.5.3. Time-temperature-concentration-shift. The influences of temperature and humidity with Eq. 16 and Eq. 18 lead to the time-temperature and time-concentration-shift principles. The consideration of the joint influences of temperature and moisture on the viscoelastic properties is achieved by integrating these two principles with the time-temperature-concentration-shift principle, which results from the assumption of thermo- and hygrorheological simplicity. The reduced time is therefore:

$$\xi = \xi(t) = \int_0^t \frac{1}{\alpha_{res}(T(,c(\tilde{\tau})))} d\tilde{\tau}, \qquad \tilde{\xi} = \xi(\tau) \tag{19}$$

α_{res} denotes the resulting shift function, which results from the individual shift due to temperature and concentration as follows:

$$\alpha_{res} = \alpha_T \alpha_c \tag{20}$$

For the time-temperature shift function a_T, the approach according to Williams, Landel and Ferry (WLF) [82] is used above the temperature T_{aT} and an Arrhenius-type approach is used below the temperature T_{aT}, as these two approaches have proven successful for many polymers as well as for the structural adhesive investigated in this project[77]:

$$\log_{10}\alpha_T = \log \alpha_T = \begin{cases} \frac{-p_{aT1}(T-T_{aT})}{-p_{aT2}+T-T_{aT}}, T > T_{aT} \\ p_{aT3}\left(\frac{1}{T} - \frac{1}{\hat{T}_{at}}\right), T \leq T_{aT} \end{cases} \tag{21}$$

In the WLF-Arrhenius approach (Equation 21), three parameters p_{aT1}, p_{aT2} and p_{aT3} occur. The value T_{aT} is a reference temperature at which the system switches between the two approaches in Equation 21 The parameter $\hat{T}_{at}$ is usually identical to the reference temperature: $\hat{T}_{at}=T_{aT}$. It is only required if the WLF approach (Equation 21) with already identified parameters is to be shifted with respect to another reference temperature $\hat{T}_{at}=T_{aT}$. For the time-concentration-shift function α_c, the authors of [81,83] use the expression analogous to the WLF equation (Equation 21) to illustrate the influence of moisture on the viscoelastic properties of a polyester resin or epoxy resin. The structural adhesive in the present project is a filled epoxy resin, which is why the following transfer of the approach according to Equation. (Equation 21) to the time-concentration-shift function ac is obvious:

$$\log \alpha_c = \begin{cases} \frac{-p_{ac1}(c-c_{ac})}{-p_{ac2}+c-c_{ac}}, c > c_{ac} \\ p_{ac3}\left(\frac{1}{c} - \frac{1}{c_{ac}}\right), c \leq c_{ac} \end{cases} \tag{22}$$

An alternative to the approaches in Equation 33 would be the following proposal in,[84] where the influence of moisture on the viscoelasticity for nylon is recorded as follows:

$$\ln \alpha_c = p_{ac1} + p_{ac2}\left(1 - \exp\left(\frac{c_{ac} - c}{p_{ac3}}\right)\right) \tag{23}$$

The following relaxation functions for normal and shear stress Rs and Rn are each assigned the Wiechert model with equilibrium chain according to Equation 13:

$$R_s(\xi_s - _s) = k_{s\infty} + \sum_{i=1}^{M} k_{si} \exp\left(-\frac{\xi_s - _s}{\tilde{\tau}_{si}}\right) \tag{24}$$

$$R_n(\xi_n - _n) = k_{n\infty} + \sum_{i=1}^{M} k_{ni} \exp\left(-\frac{\xi_n - _n}{\tilde{\tau}_{ni}}\right) \tag{25}$$

The shear and tensile relaxation time in Equation 33 and Equation 33 for summation member i are defined analogue to Equation 12 as follows:

$$\tilde{\tau}_{si} = \frac{\eta_{si}}{k_{si}}, \tilde{\tau}_{ni} = \frac{\eta_{ni}}{k_{ni}} \tag{26}$$

The reduced times in are applied analogue to Eq. 19:

$$\xi_s = \xi_s(t) = \int_0^t \frac{1}{\alpha_{res,s}(T(\tilde{\tau}), c(\tilde{\tau}))}, _s = \xi_s(\tau) \tag{27}$$

$$\xi_n = \xi_n(t) = \int_0^t \frac{1}{\alpha_{res,n}(T(\tilde{\tau}), c(\tilde{\tau}))}, _n = \xi_n(\tau) \tag{28}$$

They contain the resulting shift functions $\alpha_{res,s}$ and $\alpha_{res,n}$ for shear and normal direction:

$$\alpha_{res,s} = \alpha_{T,s}\alpha_{c,s} \tag{29}$$

$$\alpha_{res,n} = \alpha_{T,n}\alpha_{c,n} \tag{30}$$

The shift functions are applied analogue to Equation 21 and Equation 21:

$$\log \alpha_{T,s} = \begin{cases} \frac{-p_{aT1,s}(T - T_{aT,s})}{-p_{aT2,s} + T - T_{aT,s}}, T > T_{aT,s} \\ p_{aT3,s}\left(\frac{1}{T} - \frac{1}{\hat{T}_{aT,s}}\right), T \leq T_{aT,s} \end{cases} \tag{31}$$

$$\log \alpha_{T,n} = \begin{cases} \frac{-p_{aT1,n}(T - T_{aT,n})}{-p_{aT2,n} + T - T_{aT,n}}, T > T_{aT,n} \\ p_{aT3,n}\left(\frac{1}{T} - \frac{1}{\hat{T}_{aT,n}}\right), T \leq T_{aT,n} \end{cases} \tag{32}$$

$$\log \alpha_{c,s} = \begin{cases} \frac{-p_{ac1,s}(c - c_{ac,s})}{-p_{ac2,s} + c - c_{ac,s}}, c > c_{ac,s} \\ p_{ac3,s}\left(\frac{1}{c} - \frac{1}{\hat{C}_{ac,s}}\right), c \leq c_{ac,s} \end{cases} \tag{33}$$

$$\log \alpha_{c,n} = \begin{cases} \frac{-p_{c1,n}(c - c_{ac,n})}{-p_{ac2,n} + c - c_{ac,n}}, c > c_{ac,n} \\ p_{ac3,n}\left(\frac{1}{c} - \frac{1}{\hat{C}_{ac,n}}\right), c \leq c_{aT,n} \end{cases} \tag{34}$$

2.2.6. Identification, verification and validation of the model parameters

Experimentally determined material parameters are used for the final parameterisation of the previously developed models for describing viscoelasticity and damage. During parameter verification, the rheological parameters and necessary shifts for time and temperature are determined using the DMA. Technical samples are used to identify irreversible parameters for the damage model and to adjust the equilibrium spring. To ensure reliable parameter identification, all specimens are conditioned until the entire adhesive layer reaches ≥ 99% saturation, guaranteeing uniform moisture levels throughout. This conditioning time is derived from gravimetric diffusion measurements and numerical diffusion analyses. As a result, specimen size and potential differences in surface diffusion rates do not affect the material characterization. It is necessary to note that the process of scaling up the ageing results from a small coupon to a large structure should be performed with caution. In this process, the ageing of the adhesive/adherend interface should also be taken into account (see. section 4.2.1). Parameter identification and verification is the subject of other works by the authors.[61,63] The publication is currently in progress. During model validation, no further adjustments are made to the model and the previously identified parameters are applied. The identified parameters and a comprehensive verification of these parameters are documented and can be made available by the authors upon request. For this reason, the data will not be repeated here.

The validation of the developed model and the associated material parameters is the scope of this paper and is carried out by comparing the results of the creep tests on modified H-specimens with the fracture times calculated by varying the stress, temperature and moisture. Bearing and load introduction are realised via rigid bodies, which are connected to the joining parts via compatible nodes. The length of the rigid bodies corresponds to the clamping lengths of the adapters attached to the specimens. All degrees of freedom of the rigid body for the support are prevented. The rigid body for the load introduction is provided with an additional (extra) node, at which the load is introduced by the constant force F. The node is placed in the plane of symmetry. The degrees of freedom of the rigid body for load application are defined by the additional node. At the edge of the adhesive layer, with the exception of the nodes in the plane of symmetry, there is a concentration boundary condition with c_∞. The joining parts are modelled as diffusion barriers.

The thermal load is applied directly to the nodes of the adhesive layer via the material card. The FE model of the modified H-specimen is presented in Figure 3. It consists of two steel components and an adhesive layer. The adhesive layer is modelled using multiple elements across its thickness, comprising several cohesive zone element layers (shown in blue), in which damage is calculated, and adhesive elements (shown in red), which exhibit solely

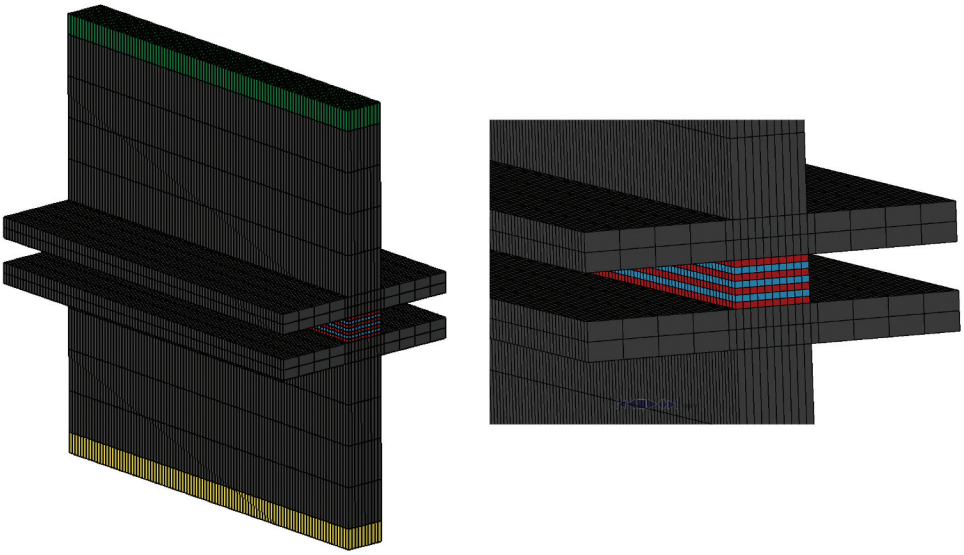

Figure 3. FE model of the modified H-specimen for the simulation calculation in LS-DYNA.

viscoelastic behaviour according to the Maxwell parameters listed in the table. The hygro-thermo-mechanical damage is calculated within the cohesive zone model according to the governing equations, as a function of temperature, creep load, and relative humidity.[85] A natural next step is to perform the full analysis with solid elements in the overlap region, enabling a more accurate representation of local triaxiality, and hygro-thermal gradients.

2.3. Experimental investigations on adhesively bonded modified H-specimens

2.3.1. Experimental series

The experimental investigations on the modified H-specimens are carried out in two separate parts. In a first test programme with a total of four test series, the influence of a variable temperature and a variable moisture concentration of the environmental air on the deformation behaviour and the load-bearing capacity of the H-specimens as a result of a quasi-static short-term load is determined. The specimens are first stored for a certain period of time at different temperature-humidity conditions in order to achieve a defined moisture content in the adhesive layer. After pre-storage, the quasi-static tensile test is carried out immediately after removal from the controlled atmosphere until the adhesive bonding fails. During the tensile tests, the machine force and the machine displacement are recorded. The results serve as a reference for determining the load levels required for the second test programme. In a second test programme with a total of four test series, the influence of a variable temperature and a variable moisture content of the environmental air on the deformation behaviour and the load-bearing

capacity of the H-specimens as a result of a quasi-static creep load is determined. In both test series, the environmental temperatures 23°C and 40°C and the relative humidities 50% and 80% are investigated.

The respective test matrices for the short-term and long-term tests performed are provided in section 2.3.4 and 2.3.5.

The specimens can be identified below by a standardised specimen designation that contains information about the type of specimen under investigation, the type of test and the environmental conditions. The exemplary specimen designation HP-KZ-23/50 first contains the type of specimen (modified HP specimen). This is followed by the type of test (KZ – short-term exposure) and the ambient conditions (23°C / 50% relative humidity).

2.3.2. Manufacturing of adhesively bonded H-specimen

The manufacturing process for the modified H-specimen is described below. Firstly, the surfaces of the parts to be bonded are prepared. The aim of this surface preparation is to increase the adhesion forces between the part to be joined and the adhesive and thus increase the static and dynamic load-bearing capacity. A high temperature and humidity in the environmental air can also favour corrosion processes on steel surfaces. Depending on the duration of exposure, this can be accompanied by an undermining of the adhesive layer in the area of the boundary layer by corrosion products (bondline corrosion). This can significantly reduce the load-bearing capacity of the bonded joint.[51] To minimise the risk of corrosion in the interface between the adhesive and the bonded part, the steel surface is pretreated with a suitable primer before the bonding process.

Before bonding, the surfaces are brushed with a wire brush to remove coarse dirt and rust and cleaned with methyl ethyl ketone (MEK). The contact surfaces to be bonded are then blasted over a large area with corundum sand to surface quality Sa 3 in accordance with EN ISO 8501–1.[86] The blasted surfaces are then cleaned again with MEK.

Finally, the primer BETAPRIME 1707 is applied with a paint roller as shown in Figure 4. The specimens coated with primer are stored for 3 hours at a temperature of 70°C to accelerate the hardening process. Moulded parts made of polyethylene (PE) and screw clamps are used to manufacture the modified H-specimens. The PE moulded parts have a T-shaped cross-section. They are used to position the parts to be joined in relation to each other and to adjust the thickness and width of the adhesive layer. First, PE moulded parts are cleaned and degreased. Then, for each specimen, two PE moulded parts are positioned between two primed T-profile sections so that they lie against the longitudinal edges of the parts to be joined. The parts to be joined and the moulded parts are then fixed in place using two screw clamps (Figure 5, left).

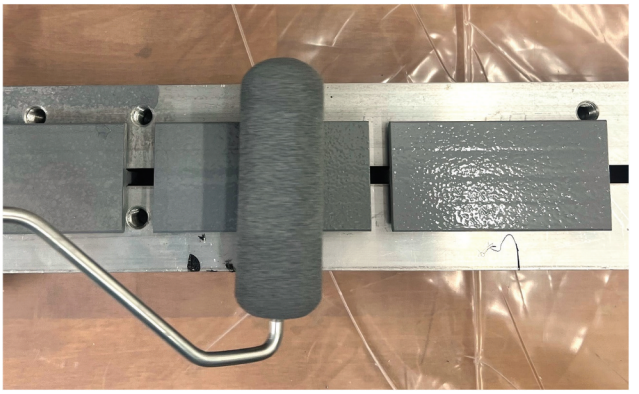

Figure 4. Priming the surfaces of the parts to be joined.

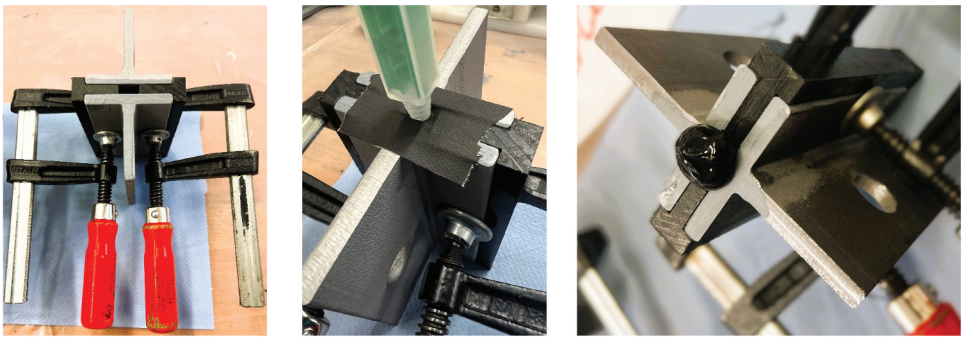

Figure 5. Left: Positioning of the T-profile sections using polyethylene moulded parts and fixing with two screw clamps; centre: Adhesive bonding by applying the adhesive at an angle of 45° to the upper end face of the joining gap; Right: formation of an adhesive bulge at both ends of the joint after the end of the adhesive application.

One end of the specimens is then covered with a piece of adhesive tape with a slit in it. The opening of the static mixer is inserted through this slit and the adhesive is injected into the adhesive joint. The static mixer is positioned at an angle of around 45° to the end face so that the adhesive wets the surface of the part to be joined immediately after leaving the mixer. This ensures that the adhesive can spread evenly from the covered end face in the longitudinal direction of the adhesive gap. The adhesive injection is completed as soon as the adhesive emerges from the underside (Figure 5, right).

2.3.3. Conditioning of the modified H-specimens

The purpose of pre-storage is to achieve complete water saturation of the adhesive layers of the specimens. Due to the small ratio of exposed surface area to adhesive volume, the process of moisture diffusion is relatively slow under the climatic conditions described above. In order to achieve

a short ageing period, the ageing boundary conditions must be adapted by increasing the ambient temperature. All specimens are therefore aged at 70°C and the respective relative humidity at which the quasi-static tensile and creep tests are subsequently carried out. The duration of ageing depends on the desired, graded water concentration (see section 2.2.2).

The climatic conditions during conditioning are monitored and documented by appropriate temperature and humidity sensors. In addition, the climatic conditions in the two chambers used for the creep tests are recorded for the entire duration of the creep tests (s. section 2.3.5). Figure 6 shows an example of the temperature and relative humidity curve in the two chambers during the conditioning and the subsequent creep test. The water absorption of the adhesive layer of the modified H-specimens is analysed using Fickian´s diffusion model presented in section 2.2, considering the effects of humidity and temperature on the saturation state. The conditioning protocol was designed to obtain a uniform and well-defined moisture state within the adhesive layer before mechanical testing. All modified H-specimens were stored under constant temperature and relative humidity for 14 days until the adhesive layer reached a minimum of 99% water saturation throughout its entire thickness. This ensures that reversible moisture-induced changes of the viscoelastic properties are fully developed and identical at all locations within the adhesive. Irreversible moisture-only damage is negligible within the time scales relevant to this study. Due to this uniform moisture state, neither diffusion gradients nor moisture transport processes are present during subsequent mechanical tests, allowing a clear separation between hygro-thermal conditioning and mechanical creep behaviour.

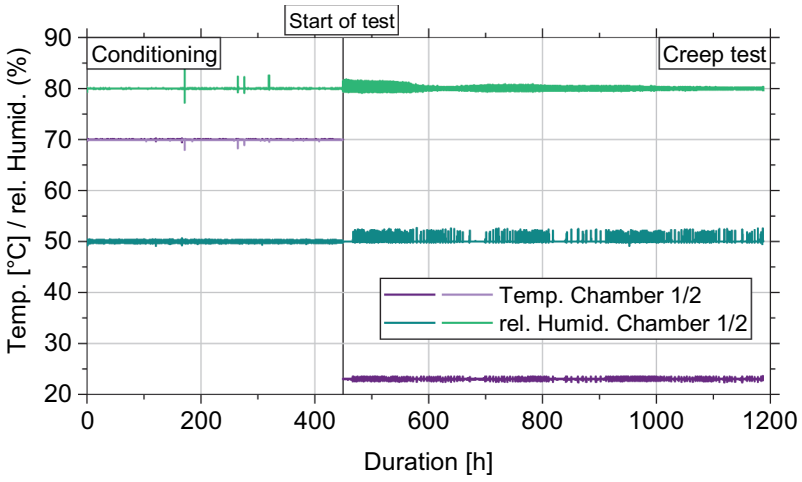

Figure 6. Exemplary representation of temperature and humidity in the two chambers over time during conditioning and creep test.

2.3.4. Short-term tensile tests on adhesively bonded H-specimen

Experimental testing of the modified H-specimen is carried out on the inspekt 250 kN universal testing machine in upright two-column design from Hegewald & Peschke with a maximum static test load of 50 kN.

A climatic test chamber from mytron Bio- und Solartechnik GmbH is used to generate the test climate. The climate chamber is positioned under the crosshead of the machine. Tension rods, to which the test specimens are connected, are inserted into the test chamber through openings at the top and bottom. The load introduction constructions are shown in Figure 7. The test force is applied on both sides by two spherical rod ends M24, each of which is joined to the ends of the test specimen by an adapter element. The adapter elements are connected to the ends of the test specimen with bolts not shown in Figure 7 via through-holes arranged there. The rod ends are attached to the fork-shaped tension rod ends of the testing machine using bolt connections. By using the rod ends, an articulated connection of the specimens to the testing machine is achieved and undesirable constraints in the specimens are avoided. As part of the test, the machine force and the machine displacement are measured and recorded using the testing machine's data acquisition software. All tests are performed in displacement-controlled mode with a constant traverse speed of 2 mm/min under defined climatic test conditions.

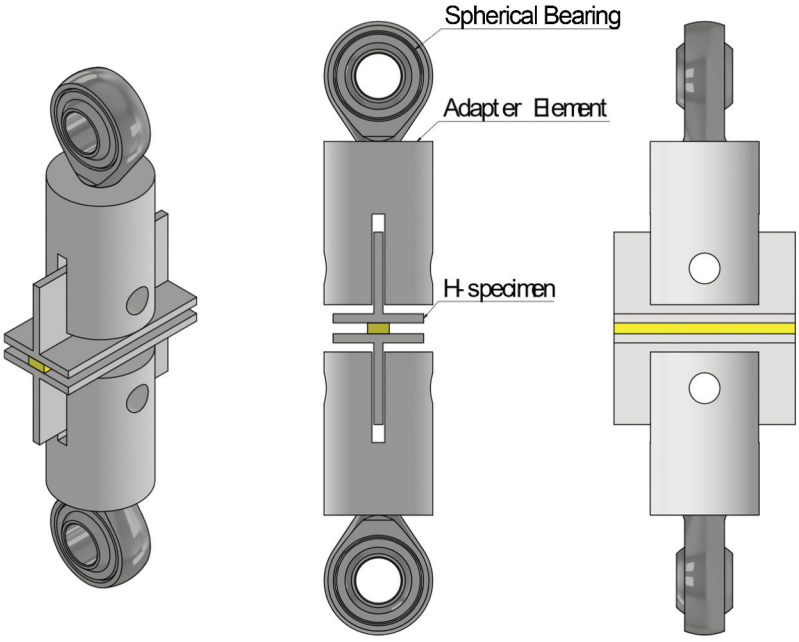

Figure 7. Schematic representation of an adhesively bonded H-specimen and the elements for adapting the specimen to the testing machine.

Table 2. Test series of the short-term tensile test on adhesively bonded H-specimens.

Test Series	Designation	Temperature	Relative Humidity	Tests
1	H-KZ-23/50	23°C	50%	3
2	H-KZ-23/80		80%	3
3	H-KZ-40/50	40°C	50%	3
4	H-KZ-40/80		80%	3

The series of tests performed with quasi-static tension test are summarised in Table 2.

2.3.5. Creep tests on adhesively bonded H-specimen

2.3.5.1. Test setup. The creep tests are carried out on the previously described, component-like modified H-specimen under constant mechanical load. Various temperature-humidity environmental conditions are investigated. The aim of the investigations is to know the influence of varying temperature-humidity environmental conditions on the deformation behaviour and the load-bearing capacity of the component-like, modified H-specimen under constant mechanical load. The tests are carried out in a test setup designed, dimensioned and manufactured for this purpose.

The test setup comprises a load application construction and a climatic chamber in which the specimens are conditioned and then tested. To introduce the creep loads to be applied, the steel frame structure shown on the left in Figure 8 is constructed and assembled from structural steel profiles. This consists of structural steel sections that are joined together to form a frame system using welded and bolted connections.

Weights are placed on the right end of the load introduction beam (HEA 160), which acts as a lever arm, during the test. The load transfer beam rests on the left-hand side in a support pocket incorporated in an HEA. On this side,

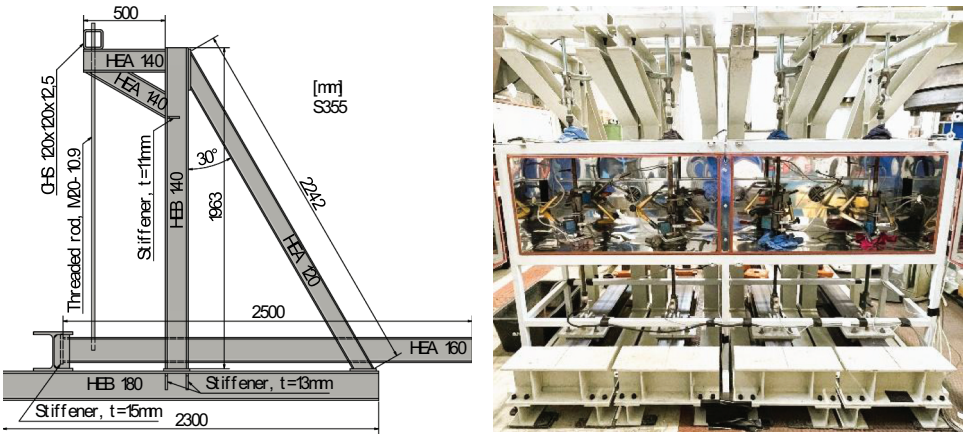

Figure 8. Left: technical drawing of the frame construction made of structural steel profiles for carrying out the creep tests; right: experimental setup of the long-term creep tests.

the load transfer beam has a welded head plate with rounded edges at both ends, which allows the beam to rotate in the pocket. In the area of the support pocket, the tension rod and an intermediate load cell are connected to the load transfer beam via a plate with an eyelet. There are joints on the top and bottom of the tension rod to compensate for eccentricities. The dead weight and the applied weights create a tensile force in the tension rod and in the installed test specimens. The four load application constructions used are decoupled from each other in order to avoid influencing other tests through premature, sudden failure of a specimen.

The climate chamber can be inserted into the steel frame construction as shown in Figure 8. Each chamber has two openings at the top and bottom through which the tension rods can be passed. When installed, the test specimens are located inside the chambers and are thus constantly exposed to the set test climate. A built-in test specimen with connected measurement technology in the climate chamber is shown in Figure 9. The relevant components of the experimental setup are marked here.

2.3.5.2. Recording of test data. The sensors installed in the climate chamber allow documentation of the relative humidity and the environmental temperature over the entire course of the test. The temperature-humidity environmental conditions correspond to those of the quasi-static tests. During the creep tests, the displacements of the test specimens and the applied creep load are also measured and documented. The existing tensile force is set and measured using a force sensor connected to the tension rod before the test begins.

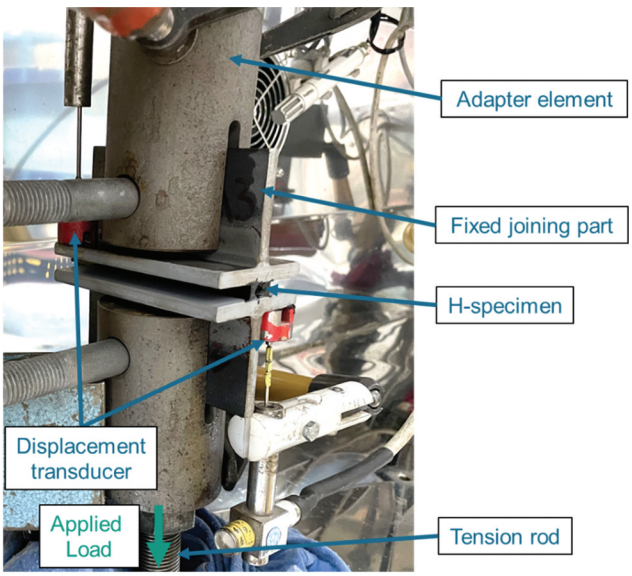

Figure 9. Built-in test specimen with connected measurement technology in the climate chamber.

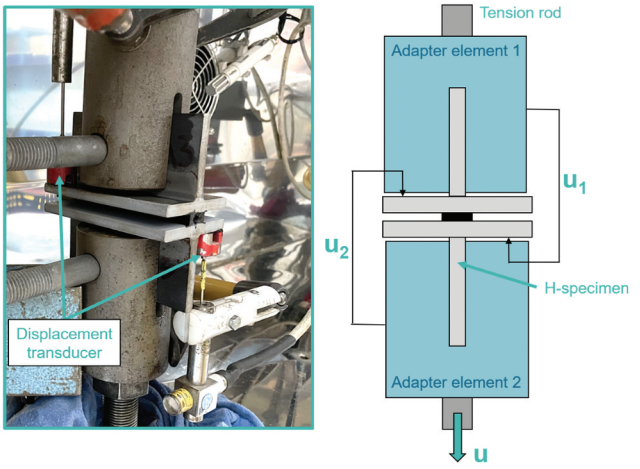

Figure 10. Measurement of the relative displacement of the two joining parts of the H-specimen via inductive displacement transducers.

The relative displacement of the two joining parts of the modified H-specimen is measured using two inductive displacement transducers. The displacement transducers used fulfil the requirements for accuracy class 1 in accordance with DIN EN ISO 9513. One base each of the displacement transducers is attached to the upper and lower specimen holder.

The upper adapter element is approximately displaceable in the direction of the applied tensile force. During the test, the lower adapter element experiences the theoretical, time-dependent deformation u. The displacement is then measured via the measuring arm, as shown in Figure 10. The relative displacement of the two joining parts can be determined from the arithmetic mean of the two displacement signals u_1 and u_2.

2.3.5.3. Test parameter and test program. The results of the quasi-static load capacity tests on the H specimens are used to determine the loads for the creep tests. Three different load levels are investigated, which differ in terms of the permanent load applied. The permanent load corresponds to a defined proportion of the quasi-static load-bearing capacity. The aim is to achieve fracture times of 24 h (load level 1), 100 h (load level 2) and 1000 h (load level 3). Two tests are carried out for each load level and environmental conditions. The series of creep tests performed with constant loading are summarised in Table 3.

3. Results

3.1. Calculated ageing times of the test specimens

Figure 11 shows the water concentrations in the centre of the adhesive layer of the modified H-specimen at different times of the ageing process as a function

Table 3. Test series of the short-term tensile test on adhesively bonded H-specimen.

Test Series	Designation	Temperature	Relative Humidity	Load level	Tests
1	H-KZ-23/50	23°C	50%	1	2
				2	2
				3	2
2	H-KZ-23/80		80%	1	2
				2	2
				3	2
3	H-KZ-40/50	40°C	50%	1	2
				2	2
				3	2
4	H-KZ-40/80		80%	1	2
				2	2
				3	2

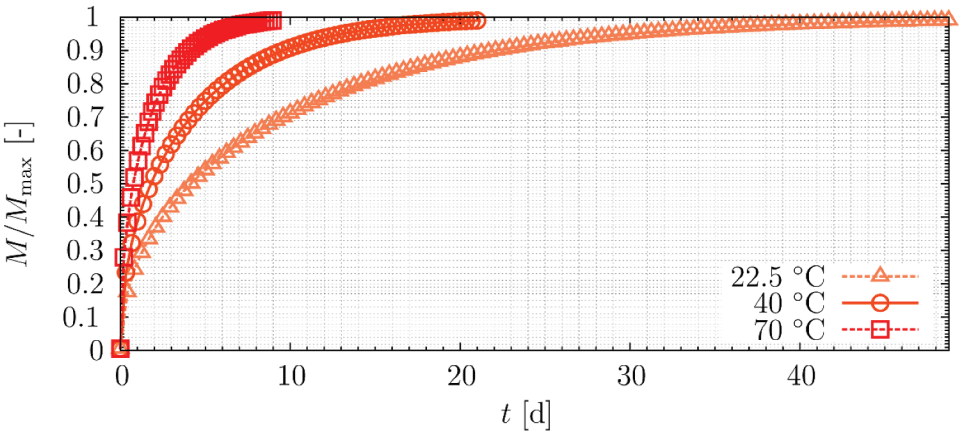

Figure 11. Water concentration over time at 22.5, 40 and 70 degrees Celsius to determine exposure duration of the H-specimen until a water concentration of 99% of the adhesive layer is reached (ageing times: 9 days at 70°C, 21 days at 40°C and 49 days at 22.5 °C).

of an environmental temperature between 22.5°C and 70°C, calculated using Equation 1

It can be seen that the increase in water concentration in the adhesive layer decreases exponentially with increasing ageing time. In addition, the ageing time decreases with increasing ambient temperature.

In addition, the distribution of the water concentration across the cross-section of the modified H-specimen as a function of the ageing time is shown in Figure 12 for the ambient temperature of 70°C as an example. The water concentrations are highest in the border area, which is adjacent to the environmental air, and decrease continuously towards the centre. The lowest water concentration is reached in the centre of the adhesive layer.

Complete saturation of the adhesive layer, which is assumed for 99% saturation, can be achieved in 49 days, 21 days or 9 days, depending on the environmental temperature under consideration. In view of the need for the

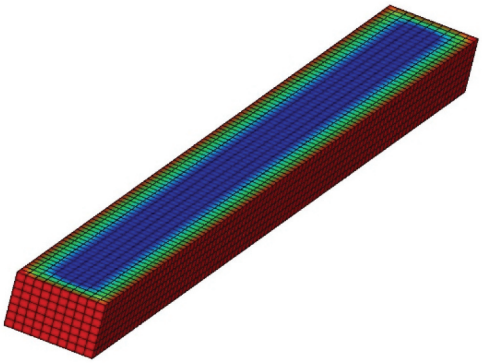

Figure 12. Distribution of the water concentration across the cross-section of the adhesive layer of the H-specimen at an unsaturated state.

shortest possible ageing period, the test specimens are aged at 70°C for 9 days. After the saturation period, the distribution or water concentration is homogeneous.

3.2. Short-term tensile tests

Figure 13 and Figure 14 show the machine force-machine displacement curves separately for the two test temperatures of 23°C and 40°C and the relative humidities of 50% and 80%. Table 4 lists the individual values and mean values of the breaking loads F_{Max} and the associated displacements u at F_{Max}.

For both levels of test humidity, the curves demonstrate linearity until shortly before maximum force is attained. With the onset of the fracture, the curves become increasingly flatter and fall rapidly after the maximum force is reached.

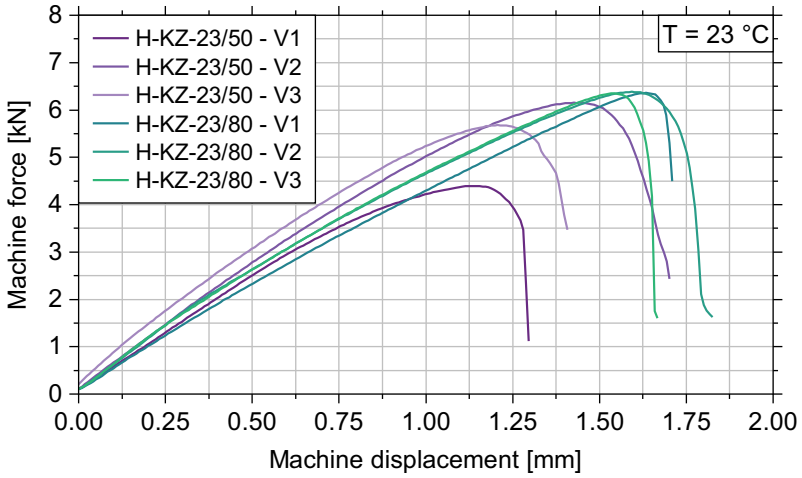

Figure 13. Machine force – machine displacement diagram of the short-term tensile tests on H-specimens at 23°C environmental temperature and 50% and 80% relative humidity.

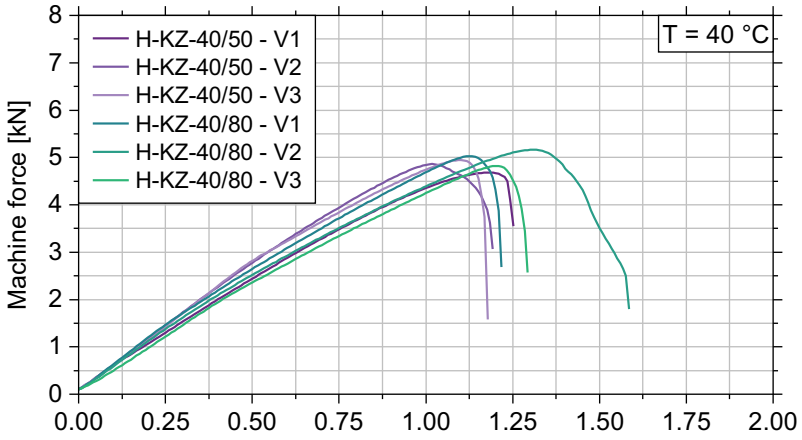

Figure 14. Machine force – machine displacement diagram of the short-term tensile tests on H-specimens at 40°C environmental temperature and 50% and 80% relative humidity.

Table 4. Failure loads and associated displacements of the quasi-static short-term tensile tests on modified H-specimens at 23°C or 40°C and 50% RH or 80% RH based on [63].

Test Series	Designation	Test Nr.	F_{Max} [kN]	u at F_{Max} [mm]
1	H-KZ-23/50	1	(4.39)	(1.22)
		2	6.16	1.43
		3	5.68	1.21
		Mean value	5.92	1.32
2	H-KZ-23/80	1	6.39	1.64
		2	6.38	1.59
		3	6.35	1.54
		Mean value	6.35	1.59
3	H-KZ-40/50	1	4.68	1.19
		2	4.86	1.09
		3	4.94	1.10
		Mean value	4.83	1.13
4	H-KZ-40/80	1	5.03	1.13
		2	5.16	1.32
		3	4.82	1.20
		Mean value	5.00	1.22

Firstly, the results for the temperature/humidity combinations 23°C / 50% RH and 23°C / 80% RH are analysed. Test V1 is not included in the following evaluation, as a large air inclusion can be recognised in the fracture surfaces of this test specimen.

The mean value of the failure load for the test boundary conditions 23°C / 50% RH is 5.92 kN. The corresponding mean displacement is 1,32 mm. At the same temperature and a humidity of 80% RH, the mean value of the failure load is 6.35 kN with a mean value of the displacement of 1.59 mm.

The curves and the failure loads at 40°C / 50% RH are within the scatter range of the results at 40°C / 80% RH. The curves tend to be lower at a test humidity of 80% RH than at a test humidity of 50% RH. As with the test temperature of 23°C, the increase in test humidity from 50% RH to 80% RH is associated with an increase in the average failure loads from 4.83 kN to 5.00

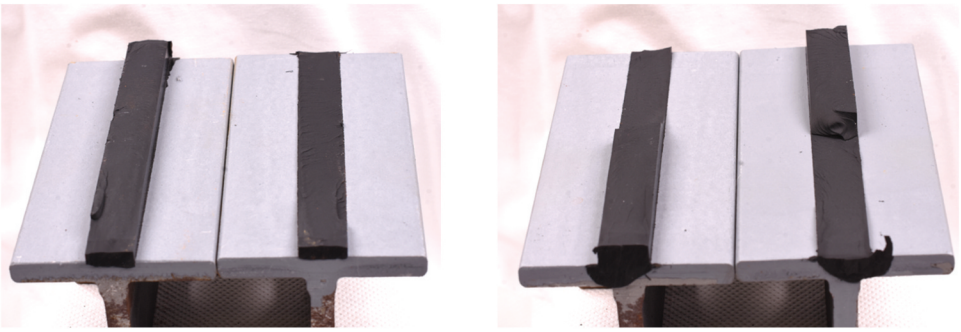

Figure 15. Quasi-static short-termin tensile tests on modified H-specimens: exemplary documentation of the fracture surfaces (left: HP-KZ-40/80–3; right: HP-KZ-23/80–3).

kN. The shift in maximum force also increases on average with increasing test humidity. For a relative humidity of 50% RH, a mean displacement of 1.13 mm can be documented. In contrast, the mean displacement at a humidity of 50% RH is 1.20 mm.

Ductile shear failure is observed for all specimens. Figure 15 shows exemplary photos of the fracture surfaces of test specimens H-KZ-40/80–3 and H-KZ23/80–3. Cohesive failure of the bonded joint is evident for all specimens. The fracture surface was characterised either by a flat shape (Figure 15, left) or by a stepped shape (Figure 15, right).

3.3. Long-term creep tests

The fracture times determined in creep tests on modified H specimens under constant, combined mechanical, thermal and hygro stress are shown in Figure 16. The x-axis represents the time taken for the specimens to fracture in hours. The y-axis shows the nominal tensile normal stresses in the adhesive layer in Megapascal during the long-term test. The associated loads are defined on the basis of the results of static tensile tests. The fracture times determined are between 0.4 h and 930 h, depending on the applied tensile normal stress. The tests showed that for a stress of less than 1.5 MPa, no failure of the test specimens could be achieved for a period from 930 hours up to 1600 hours. The tests were therefore terminated before failure and included in the diagram for the sake of completeness. The tests are marked accordingly in the diagram. They are also not part of the further evaluation.

The results show that the fracture times of the test specimens decrease with increasing applied tensile normal stress. At the same tensile normal stress and relative humidity, the fracture times tend to increase with decreasing temperature. Furthermore, it can be observed that the fracture times tend to decrease with increasing relative humidity at the same tensile normal stress and constant temperature.

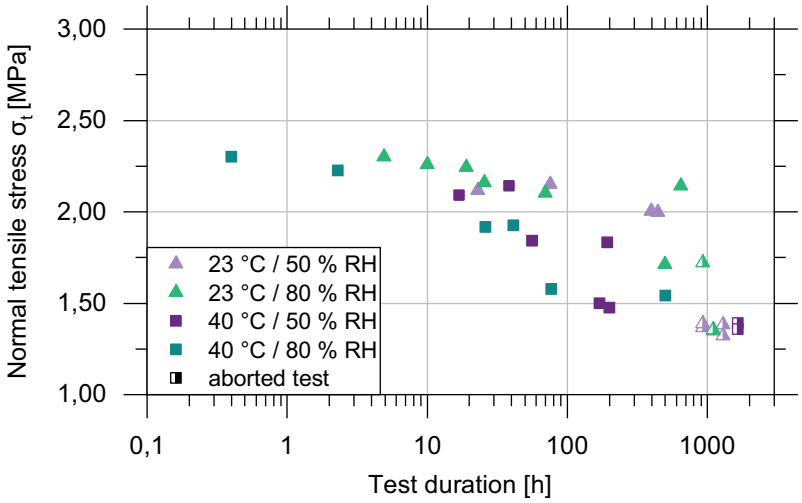

Figure 16. Tensile normal tension-failure time diagram of creep tests on modified H-specimen under constant, combined mechanical, thermal and hygro loading.

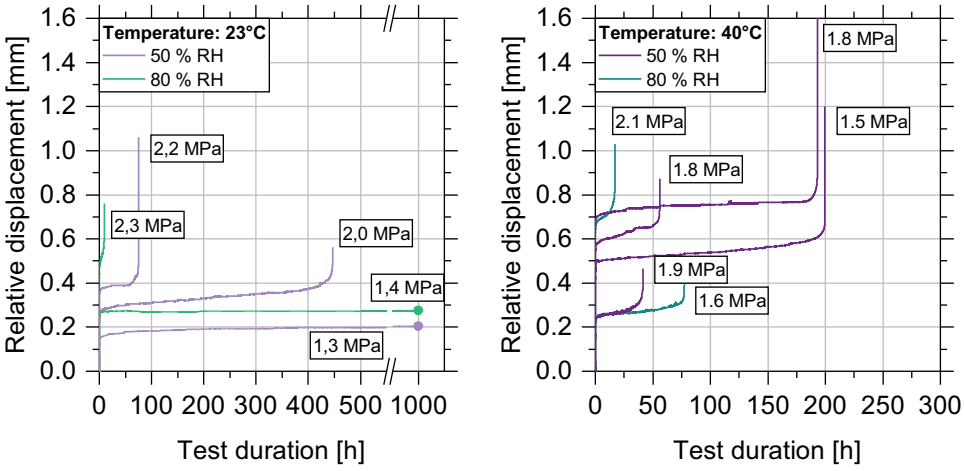

Figure 17. Relative displacement-failure time diagram of creep tests on modified H-specimen under constant, combined mechanical, thermal and hygro loading.

Figure 17 shows additionally determined relative displacements of the bonded parts during the test as a function of the applied nominal tensile stress in the adhesive layer, separately for the test temperatures 23°C (left) and 40°C (right).

4. Discussion

4.1. Influence of environmental conditions

Temperature and humidity are among the main environmental influences that can affect the behaviour of adhesive bonds. Both factors have an independent

effect on the properties of the adhesive and the bond. In addition, they can reinforce each other and, when combined, lead to more complex changes than when considered in isolation.

4.1.1. Short-term load bearing behaviour

The test results of the short-term tensile tests for the temperature/humidity combinations 23°C / 50% RH and at 23°C / 80% RH show that the failure loads are higher than at 40°C and the equivalent test humidity. At a temperature of 23°C and an air humidity of 50% RH, the average failure load in the short-term tensile tests is 23% higher compared to the test temperature of 40°C and the same air humidity. For a relative humidity of 80%, the average failure load in the short-term tensile tests increases by 27% as a result of reducing the test temperature from 40°C to 23°C. The drop in the maximum load-bearing capacity as a result of increasing the test temperature from 23°C to 40°C can be primarily explained by the approach of the test temperature to the glass transition temperature of the adhesive. The increase in deformation upon reaching the failure load can also be explained by this.

In the range of the glass transition temperature, the stiffness and strength of adhesives decrease significantly.[87] According to,[87] another reason for the decrease in failure load as a result of higher temperature may be temperature-related expansion differences between the bonded parts and the adhesive layer due to different expansion coefficients.

Furthermore, it can be seen that the maximum load-bearing capacities for both temperatures investigated increase by 7.3% (23 °C) and 4.5% (40 °C) with increasing humidity. In,[88] the impact of relative humidity on the moisture cross-linking of polyurethane adhesives is shown. Using FTIR spectroscopy, it was shown that higher relative humidities (65–85%) significantly increases the reaction rate. DFT calculations show that water clusters greatly reduce the activation energy, which accelerates the crosslinking process and explains slight increases in load-bearing capacity, especially in the context of short ageing times.

4.1.2. Long-term load bearing behaviour

The results of the long-term creep tests on modified H specimens under defined climatic conditions, which form the basis for the model validation in section 4.2, show a clear influence of temperature and relative humidity on the creep behaviour of the bonded joints. At 23°C and 50% relative humidity, the longest test times to failure are achieved on average with the same applied tensile normal stress.

As the temperature rises to 40°C, there is a significant reduction in the test times compared to the tests at 23°C and the same tensile standard stress, regardless of the humidity. It can thus be deduced that the applicable stresses for a given test time at an ambient temperature of 23°C are significantly greater

than at a temperature of 40°C. This is primarily due to the test boundary conditions being close to the adhesive's glass transition temperature. This applies in particular to long durations in which the temperature-induced degradation of the adhesive properties increases. Furthermore, it can be observed that the fracture times tend to decrease with increasing relative humidity at the same tensile normal stress and constant temperature. The negative influence of absorbed moisture on the strength and stiffness of adhesives with long-term exposure is described in the literature for EP adhesives[89–91] and for PU adhesives.[92] It is important to note that moisture-induced ageing comprises both reversible and irreversible mechanisms. Irreversible degradation caused solely by moisture proceeds very slowly and plays no practical role within the present investigation. The dominant influence is the reversible change of viscoelastic properties, which depends directly on the water content. Since all specimens were tested in a fully saturated and spatially uniform moisture state, the mechanical responses in sections 3 and 4 are not affected by ongoing diffusion processes. This allows direct attribution of the observed behaviour to temperature and mechanical load, while reversible moisture effects are already fully incorporated in the initial material state.

The reason for this is the absorption of moisture according to Fickian´s law, which leads to hydroplasticitation and possibly swelling stresses. Another reason is hydrolysis. During hydrolysis, water molecules attack chemical bonds in the polymer network. Examples include ester, urethane or amide bonds, which occur in many structural adhesives (e.g. epoxy resins, polyurethanes). Both of these negative influencing factors are preferred by an increased ambient temperature and exposure times.[87,93]

4.2. Validation of the numerical model

In Figure 18 the experimentally determined fracture times of the creep tests on modified H-specimen are shown as a function of the level of tensile stress, the temperature and the relative environmental humidity. To validate the developed calculation model, the experimental data points are compared with the fracture times determined by calculation. The validation results with the final parameterised material model show a good agreement between simulation and experiment. The short-term experiments were also recalculated with good agreement between experiment and simulation as part of the underlying research project. However, for reasons of space, they were not included in the paper.

The agreement between simulation and experiment can be regarded as satisfactory and practical, particularly when considering that, for example, the experimental data at 40 °C/80% RH encompass the data points obtained at 40 °C/50% RH, and that the simulation results lie within the same order of magnitude while preserving physical plausibility.

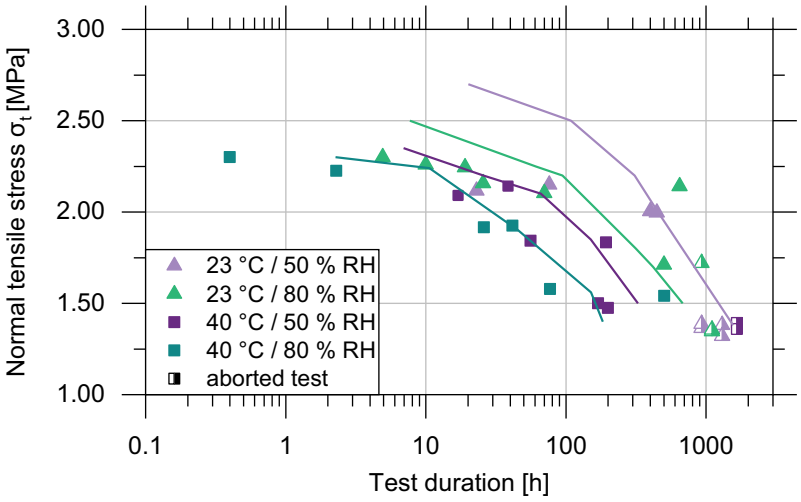

Figure 18. Simulation and experiment: validation calculation. Tensile normal tension-failure creep tests on modified H-specimen under constant, combined mechanical, thermal and hygro loading [63].

The inflection point is of particular importance, as it marks the transition between the dominant influences of creep damage and hygro damage. Especially at higher creep load levels, the fracture times are less affected by hygro damage than at very low load levels, where saturation effects as well as reversible and irreversible hygro ageing become decisive. The pronounced change in slope becomes more distinct at higher temperatures and under stronger hygro influences. A more detailed discussion of these effects can be found in.[85] It should be noted that the parameters identified for the hygro-thermo-mechanical damage model presented here, as well as the reversible viscoelastic parameters, were determined based on DMA investigations and experimental studies conducted on significantly smaller specimens. The experimentally and numerically determined results of the tests at a test temperature of 23°C and relative humidity of 50% show a high degree of consistency. The deviations between the experiment and the numerical results for the remaining three boundary conditions are small but noticeable. The deviations can generally be attributed to uncertainties in the transfer of material parameters from substance and small specimens to larger specimen geometries.

4.2.1. Opportunities and necessary boundary conditions

In addition, Figure 19 shows the cohesive zones of an exemplary adhesive layer, where the various forms if damage are calculated. In the example shown, which is intended to demonstrate the capabilities of the developed model, no conditioning took place. At the start of the test, the specimen is subjected to a creep load and exposed to a temperature of 23°C and a humidity of 80% RH.

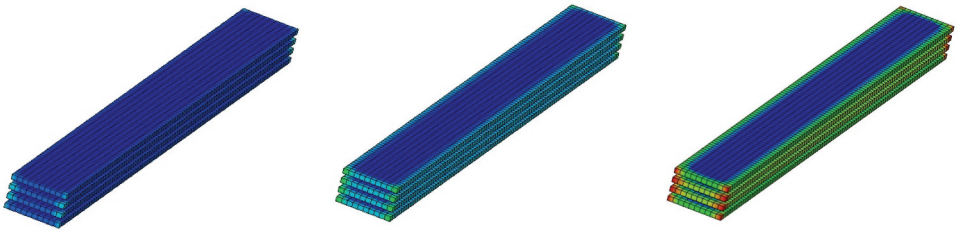

Figure 19. Results of the numerical simulation of moisture damage (left), creep damage (centre) and total damage (right) [63].

The left figure illustrates the hygro damage, the middle figure the creep damage, and the right figure the total damage D_{ca}, represented as the sum according to Equation 9 The color gradients from blue to red in the simulation indicate the magnitude of the damage values. Depending on the onset of the mechanical load or the location within the adhesive layer at which the damage values are evaluated, the influences vary in magnitude. For longer saturation times, hygro effects become more pronounced, whereas in dry environments, creep damage predominates.

Figure 20 illustrates the damage contributions from hygro and mechanical effects in an outer element and a central element, extracted from the simulation shown in Figure 19 at 23°C and 80% relative humidity, with fracture occurring after 10 hours. It is clearly evident that in an outer element the hygro influences are significantly higher and the overall damage greater than in a central element, which was exposed to only minimal moisture.

The modelling framework developed in this study is focused on the bulk adhesive layer. Interfacial behaviour, including primer-dependent or

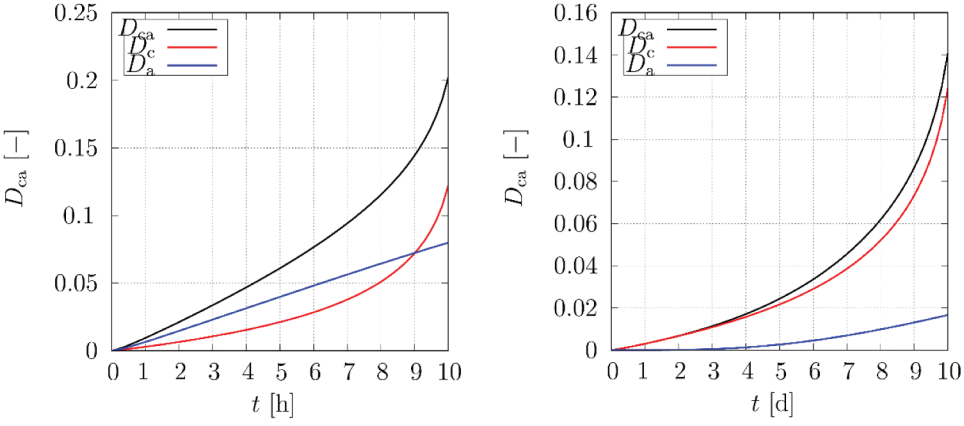

Figure 20. Illustration of the influence of damage calculations: left: outer element of the adhesive layer with significant influence of ageing damage; right: damage behaviour dominated by creep damage: element in the middle of the adhesive layer with the specimen not fully saturated and taking into account advanced reversible and irreversible ageing damage due to water diffusion.

substrate-dependent mechanisms, differs fundamentally from bulk behaviour and would require a dedicated experimental programme involving alternative adhesives that predominantly fail at the interface. The adhesive chosen for this project exhibits failure within the adhesive layer, ensuring consistency between substance-level characterisation (e.g., DMA), technological specimens, and structural tests. While the underlying theoretical model can in principle be extended to partially saturated regions or interface-dominated damage, such extensions fall outside the scope of the present work and constitute promising directions for future research.

4.3. Conclusions

In general, the use of a physically motivated constitutive and lifetime prediction model, in conjunction with material parameters identified from dynamic mechanical analysis (DMA) and technological specimen testing, enables accurate and reliable lifetime simulations of large-scale structural components in steel construction and plant engineering. The validated modelling framework allows for an optimized application of adhesive joints, targeted material reduction, and the safe implementation of lightweight design concepts over a prescribed service life.

The applicability of the model is broad and transferable, ranging from long-term durability and creep lifetime predictions to short-term dynamic analyses, including impact and crash simulations. The framework accounts not only for creep-induced damage under arbitrary mechanical loading histories, but also for transient environmental boundary conditions such as temperature variations and moisture exposure. Temperature effects influence both the mechanical response and the diffusion kinetics of the material, which are described by experimentally identified parameters covering saturated and unsaturated concentration states.

In addition, hygroscopic effects, separated into reversible and irreversible degradation mechanisms, are incorporated and shown to significantly affect the mechanical strength and damage evolution. These modelling capabilities are demonstrated in particular by the validation of the creep lifetime predictions presented in this study. Furthermore, the framework is extensible and may be adapted to incorporate cyclic fatigue loading or alternative environmental media in place of, or in addition to, pure moisture exposure.

Acknowledgments

The research project IGF-Nr. 21555 N / P 1496 from the Research Association for Steel Application (FOSTA), Düsseldorf, was supported by the Federal Ministry of Economic Affairs and Energy through the German Federation of Industrial Research Associations (AiF) as part of the programme for promoting industrial cooperative research (IGF) on the basis of a decision by the German Bundestag.

Author contributions

CRediT: **Jannis Damm:** Conceptualization, Formal analysis, Investigation, Methodology, Project administration, Supervision, Visualization, Writing – original draft, Writing – review & editing; **Thomas Ummenhofer:** Conceptualization, Funding acquisition; **Matthias Albiez:** Conceptualization, Funding acquisition, Project administration, Writing – review & editing; **Gerson Meschut:** Conceptualization, Funding acquisition; **Sascha Sander:** Investigation, Project administration, Supervision; **Dominik Teutenberg:** Project administration, Writing – review & editing; **Fabian Kötz:** Conceptualization, Formal analysis, Methodology, Project administration, Software, Validation, Visualization, Writing – original draft, Writing – review & editing.

Disclosure statement

No potential conflict of interest was reported by the author(s).

ORCID

Jannis Damm http://orcid.org/0000-0001-6185-0437
Matthias Albiez http://orcid.org/0000-0002-0475-7153

References

[1] Cavezza, F.; Boehm, M.; Terryn, H.; Hauffman, T. A Review on Adhesively Bonded Aluminium Joints in the Automotive Industry. *Metals* 2020, *10*, 730. DOI: 10.3390/met10060730.
[2] Tserpes, K. Adhesive Bonding of Aircraft Structures. In *Revolutionizing Aircraft Materials and Processes*, Pantelakis, S. Tserpes, K., Eds.; Springer International Publishing: Cham, 2020; pp. 337–357. DOI: 10.1007/978-3-030-35346-9_12.
[3] Silva, L. F. M.; Öchsner, A.; Adams, R. D. *Handbook of Adhesion Technology*; Springer: Heidelberg, 2011.
[4] Barnes, T. A.; Pashby, I. R. Joining Techniques for Aluminium Spaceframes Used in Automobiles. *J. Mater. Process. Technol.* 2000, *99*, 72–79. DOI: 10.1016/S0924-0136(99)00361-1.
[5] Zhang, Q.; Sekol, R. C.; Zhang, C.; Li, Y.; Carlson, B. E. Joining Lithium-Ion Battery Tabs Using Solder-Reinforced Adhesive. *J. Manuf. Sci. Eng.* 2019, *141*, 044502. DOI: 10.1115/1.4042842.
[6] Bucak, Ö.; Hagl, A. Kleben im Bauwesen – gestern, heute, morgen – Allgemeine Übersicht und Ausblick auf die Forschung im Konstruktiven Glasbau an der Fachhochschule München (FHM). *Stahlbau* 2006, *75*, 499–507. DOI: 10.1002/stab.200610053.
[7] da Silva, L. F. M.; Das Neves, P. J. C.; Adams, R. D.; Spelt, J. K. Analytical Models of Adhesively Bonded Joints—Part I: Literature Survey. *Int. J. Adhes. Adhes.* 2009, *29*, 319–330.
[8] da Silva, L. F. M.; Das Neves, P. J. C.; Adams, R. D.; Wang, A.; Spelt, J. K. Analytical Models of Adhesively Bonded Joints—Part II: Comparative Study. *Int. J. Adhes. Adhes.* 2009, *29*, 331–341.

[9] Albiez, M.; Vallée, T.; Fricke, H.; Ummenhofer, T. Adhesively Bonded Steel Tubes — Part I: Experimental Investigations. *Int. J. Adhes. Adhes.* 2019, *90*, 199–210. DOI: 10.1016/j.ijadhadh.2018.02.005.

[10] Albiez, M.; Vallée, T.; Ummenhofer, T. Adhesively Bonded Steel Tubes – Part II: Numerical Modelling and Strength Prediction. *Int. J. Adhes. Adhes.* 2019, *90*, 211–224. DOI: 10.1016/j.ijadhadh.2018.02.004.

[11] Dragoni, E.; Goglio, L. Adhesive Stresses in Axially-Loaded Tubular Bonded Joints – Part I: Critical Review and Finite Element Assessment of Published Models. *Int. J. Adhes. Adhes.* 2013, *47*, 35–45. DOI: 10.1016/j.ijadhadh.2013.09.009.

[12] Vaziri, A.; Nayeb-Hashemi, H.; Hamidzadeh, H. R. Experimental and Analytical Investigations of the Dynamic Response of Adhesively Bonded Single Lap Joints. *J. Vib. Acoust.* 2004, *126*, 84. DOI: 10.1115/1.1596550.

[13] Vaziri, A.; Nayeb-Hashemi, H. Dynamic Response of Tubular Joints with an Annular Void Subjected to a Harmonic Axial Load. *Int. J. Adhes. Adhes.* 2002, *22*, 367–373.

[14] Vaziri, A.; Nayeb-Hashemi, H. 01 12 Dynamic Response of Tubular Joints with an Annular Void Subjected to a Harmonic Torsional Load Proceedings of the Institution of Mechanical Engineers, Part K: Journal of Multi-body Dynamics. In, 2002; Vol. 216 4, pp 361–370. DOI: 10.1243/146441902320992455.

[15] Vaziri, A.; Hamidzadeh, H. R.; Nayeb-Hashemi, H. 01 12 Dynamic Response of Adhesively Bonded Single-Lap Joints with a Void Subjected to Harmonic Peeling Loads Proceedings of the Institution of Mechanical Engineers, Part K: Journal of Multi-body Dynamics. In, 2001; Vol. 215 4, pp 199–206. DOI: 10.1243/1464419011544475.

[16] He, S.; Rao, M. D. Vibration Analysis of Adhesively Bonded Lap Joint, Part I: Theory. *J. Sound Vibr.* 1992, *152*, 405–416. DOI: 10.1016/0022-460X(92)90478-G.

[17] Rao, M. D.; He, S. Vibration Analysis of Adhesively Bonded Lap Joint, Part II: Numerical Solution. *J. Sound Vibr.* 1992, *152*, 417–425. DOI: 10.1016/0022-460X(92)90479-H.

[18] Albiez, M.; Damm, J.; Ummenhofer, T.; Ehard, H.; Schuler, C.; Kaufmann, M. Hybrid Joining of Jacket Structures for Offshore Wind Turbines – Validation Under Static and Dynamic Loading at Medium and Large Scale. *Eng. Structu. Res.* 2022, *252*, 113595. DOI: 10.1016/j.engstruct.2021.113595.

[19] Albiez, M.; Damm, J.; Ummenhofer, T.; Kaufmann, M.; Vallée, T.; Myslicki, S. Hybrid Joining of Jacket Structures for Offshore Wind Turbines – Determination of Requirements and Adhesive Characterisation. *Eng. Structu. Res.* 2022, *259*, 114186. DOI: 10.1016/j.engstruct.2022.114186.

[20] Damm, J.; Ummenhofer, T.; Albiez, M.; Göddecke, J.; Meschut, G.; Kötz, F. Experimental and Numerical Investigation of the Damping Properties of Adhesively Bonded Tubular Steel Joints. *J. Adhes.* 2023. DOI: 10.1080/00218464.2023.2178909.

[21] Damm, J.; Ummenhofer, T.; Albiez, M. Influence of Damping Properties of Adhesively Bonded Joints on the Dynamic Behaviour of Steel Structures: Numerical Investigations. *J. Adhes.* 2022, *98*, 934–962. DOI: 10.1080/00218464.2020.1865161.

[22] Damm, J.; Albiez, M. Damping Properties of Large-Scale Overlap Joints Bonded with Epoxy Hybrid Resin or Polyurethanes: Experimental Characterisation and Analytical Description. *Polymers* 2023, *15*, 1102. DOI: 10.3390/polym15051102.

[23] Boretzki, J.; Albiez, M.; Damm, J.; Ummenhofer, T. Fatigue Behaviour of Hybrid Grouted Joints Under Axial Loading. *Ce. Papers.* 2023, *6*, 1151–1156. DOI: 10.1002/cepa.2425.

[24] Boretzki, J.; Albiez, M. Static Strength and Load Bearing Behaviour of Hybrid Bonded Bolted Joints: Experimental and Numerical Investigations. *J. Adhes.* 2023, *99*, 606–631. DOI: 10.1080/00218464.2022.2033619.

[25] Yokozeki, K.; Hisazumi, K.; Vallée, T.; Evers, T.; Ummenhofer, T.; Boretzki, J. Hybrid Joints Consisting of Pre-Tensioned Bolts and a Bonded Connection—A Comprehensive Review Part I: Local Approach. *Int. J. Adhes. Adhes.* 2024, *132*, 103713. DOI: 10.1016/j.ijadhadh.2024.103713.
[26] Kasper, Y.; Albiez, M.; Ummenhofer, T.; Mayer, C.; Meier, T.; Choffat, F. Application of Toughened Epoxy-Adhesives for Strengthening of Fatigue-Damaged Steel Structures. *Construct. Build. Mater.* 2021, *275*, 121579. DOI: 10.1016/j.conbuildmat.2020.121579.
[27] Kasper, Y. J. Auslegung von Verstärkungen ermüdungsgeschädigter Stahlbauteile mit aufgeklebten Faserverbundwerkstoffen. 2023. DOI: 10.5445/IR/1000157204.
[28] Ehrenstein, G. W.; Pongratz, S. *Resistance and Stability of Polymers*; Hanser Publishers: Munich, 2013.
[29] Struik, L. C. E. Physical Aging in Plastics and Other Glassy Materials. *Polym. Eng. Sci.* 1977, *17*, 165–173. DOI: 10.1002/pen.760170305.
[30] Struik, L. C. E. *Physical Aging in Amorphous Polymers and Other Materials*; Elsevier: Amsterdam, 1978.
[31] Hutchinson, J. M. Physical Aging of Polymers. *Prog. Polym. Sci.* 1995, *20*, 703–760. DOI: 10.1016/0079-6700(94)00001-I.
[32] Katnam, K. B.; Sargent, J. P.; Crocombe, A. D.; Khoramishad, H.; Ashcroft, I. A. Characterisation of Moisture-Dependent Cohesive Zone Properties for Adhesively Bonded Joints. *Eng. Fract. Mech.* 2010, *77*, 3105–3119. DOI: 10.1016/j.engfracmech.2010.08.023.
[33] Wapner, K.; Stratmann, M.; Grundmeier, G. In situ Infrared Spectroscopic and Scanning Kelvin Probe Measurements of Water and Ion Transport at Polymer/Metal Interfaces. *Electrochim. Acta* 2006, *51*, 3303–3315. DOI: 10.1016/j.electacta.2005.09.024.
[34] Vlasak, R.; Klueppel, I.; Grundmeier, G. Combined EIS and FTIR–ATR Study of Water Uptake and Diffusion in Polymer Films on Semiconducting Electrodes. *Electrochim. Acta* 2007, *52*, 8075–8080. DOI: 10.1016/j.electacta.2007.07.003.
[35] Adams, R. D.; Cowap, J. W.; Farquharson, G.; Margary, G. M.; Vaughn, D. The Relative Merits of the Boeing Wedge Test and the Double Cantilever Beam Test for Assessing the Durability of Adhesively Bonded Joints, with Particular Reference to the Use of Fracture Mechanics. *Int. J. Adhes. Adhes.* 2009, *29*, 609–620. DOI: 10.1016/j.ijadhadh.2009.02.010.
[36] Bond, D. A.; Smith, P. A. Modeling the Transport of Low-Molecular-Weight Penetrants Within Polymer Matrix Composites. *Appl. Mech. Rev.* 2006, *59*, 249–268. DOI: 10.1115/1.2202873.
[37] Comyn, J. *Adhesion Science*, 2nd ed.; Royal Society of Chemistry: Cambridge, 2021.
[38] Mubashar, A.; Ashcroft, I. A.; Critchlow, G. W.; Crocombe, A. D. Moisture Absorption–Desorption Effects in Adhesive Joints. *Int. J. Adhes. Adhes.* 2009, *29*, 751–760. DOI: 10.1016/j.ijadhadh.2009.05.001.
[39] Possart, W. *Adhesive Joints: Ageing and Durability of Epoxies and Polyurethanes*; John Wiley & Sons, Incorporated: Newark, 2019.
[40] Wahab, M. M. A.; Ashcroft, I. A.; Crocombe, A. D.; Shaw, S. J. Diffusion of Moisture in Adhesively Bonded Joints. *J. Adhes.* 2001, *77*, 43–80. DOI: 10.1080/00218460108030731.
[41] Ashcroft, I. A.; Wahab, M. M. A.; Crocombe, A. D. Predicting Degradation in Bonded Composite Joints Using a Semi-Coupled Finite-Element Method. *Mech. Adv. Mater. Struct.* 2003, *10*, 227–248. DOI: 10.1080/15376490306744.
[42] Crocombe, A. D.; Hua, Y. X.; Loh, W. K.; Wahab, M. A.; Ashcroft, I. A. Predicting the Residual Strength for Environmentally Degraded Adhesive Lap Joints. *Int. J. Adhes. Adhes.* 2006, *26*, 325–336. DOI: 10.1016/j.ijadhadh.2005.04.003.
[43] Liljedahl, C. D. M.; Crocombe, A. D.; Wahab, M. A.; Ashcroft, I. A. Modelling the Environmental Degradation of Adhesively Bonded Aluminium and Composite Joints

Using a CZM Approach. *Int. J. Adhes. Adhes.* 2007, *27*, 505–518. DOI: 10.1016/j.ijadhadh.2006.09.015.

[44] Friedland, R.; Rabe, U.; Depollier, L. *Alterungsprogression in Klebverbunden Unter Komplexer Beanspruchung (Abschlussbericht Zum IGF-Vorhaben Nr. 17458 N, FOSTA P 955)*; Forschungsvereinigung Stahlanwendung e.V: Düsseldorf, 2015.

[45] Han, X.; Crocombe, A. D.; Anwar, S. N. R.; Hu, P. The Strength Prediction of Adhesive Single Lap Joints Exposed to Long Term Loading in a Hostile Environment. *Int. J. Adhes. Adhes.* 2014, *55*, 1–11. DOI: 10.1016/j.ijadhadh.2014.06.013.

[46] Sander, S.; Meschut, G.; Kroll, U.; Matzenmiller, A. Methodology for the Systematic Investigation of the Hygrothermal-Mechanical Behavior of a Structural Epoxy Adhesive. *Int. J. Adhes. Adhes.* 2022, *113*, 103072. DOI: 10.1016/j.ijadhadh.2021.103072.

[47] Pethrick, R. A. Design and Ageing of Adhesives for Structural Adhesive Bonding – a Review Proceedings of the Institution of Mechanical Engineers, Part L: Journal of Materials: Design and Applications. In, 2015; Vol. 229 5, pp 349–379. DOI: 10.1177/1464420714522981.

[48] Ashcroft, I. A.; Wahab, M. M. A.; Crocombe, A. D.; Hughes, D. J.; Shaw, S. J. The Effect of Environment on the Fatigue of Bonded Composite Joints. Part 1: Testing and Fractography. *Compos. Appl. Sci. Manuf.* 2001, *32*, 45–58. DOI: 10.1016/S1359-835X(00)00131-7.

[49] Wahab, M. M. A.; Ashcroft, I. A.; Crocombe, A. D.; Hughes, D. J.; Shaw, S. J. The Effect of Environment on the Fatigue of Bonded Composite Joints. Part 2: Fatigue Threshold Prediction. *Compos. Appl. Sci. Manuf.* 2001, *32*, 59–69. DOI: 10.1016/S1359-835X(00)00132-9.

[50] Hua, Y.; Crocombe, A. D.; Wahab, M. A.; Ashcroft, I. A. Continuum Damage Modelling of Environmental Degradation in Joints Bonded with EA9321 Epoxy Adhesive. *Int. J. Adhes. Adhes.* 2008, *28*, 302–313. DOI: 10.1016/j.ijadhadh.2007.08.005.

[51] Habenicht, G. K. *Grundlagen, Technologien, Anwendungen. 6. Aktualisierte Auflage*; Springer Berlin Heidelberg: Berlin, Heidelberg, 2009. DOI: 10.1007/978-3-540-85266-7 .

[52] Han, X.; Crocombe, A. D.; Anwar, S. N. R.; Hu, P.; Li, W. D. The Effect of a Hot–Wet Environment on Adhesively Bonded Joints Under a Sustained Load. *J. Adhes.* 2014, *90*, 420–436. DOI: 10.1080/00218464.2013.853176.

[53] European Organisation for Technical Assessment (EOTA) 09. 2018. EAD 090010-00-0404: Bonded glazing kits and bonding sealants.

[54] Meschut, G.; Schwarzkopf, G.; Matzenmiller, A.; Nelson, A.; Mayer, B.; Brede, M. *Numerische Modellierung Und Kennwertermittlung Für Das Versagensverhalten Hyperelastischer Klebverbindungen*: 2019. (FOSTA P 1086, IGF Nr. 18716 N); Düsseldorf: 2019).

[55] Marques, S. P. C.; Creus, G. J. *Computational Viscoelasticity*; Springer Berlin Heidelberg: Berlin, Heidelberg, 2012. DOI: 10.1007/978-3-642-25311-9.

[56] Simo, J. C. On a Fully Three-Dimensional Finite-Strain Viscoelastic Damage Model: Formulation and Computational Aspects. *Comput. Methods Appl. Mech. Eng.* 1987, *60*, 153–173. DOI: 10.1016/0045-7825(87)90107-1.

[57] Kaliske, M.; Rothert, H. Formulation and Implementation of Three-Dimensional Viscoelasticity at Small and Finite Strains. *Comput. Mech.* 1997, *19*, 228–239. DOI: 10.1007/s004660050171.

[58] Simo, J. C. *Computational Inelasticity*; Springer New York: New York, NY, 2000.

[59] Holzapfel, G. A. *Nonlinear Solid Mechanics: A Continuum Approach for Engineering. Repr*; Wiley: Chichester Weinheim, 2010.

[60] Menard, K. P.; Menard, N. R. *Dynamic Mechanical Analysis*, 3rd ed.; Boca Raton: CRC Press, 2020. DOI: 10.1201/9780429190308.

[61] Damm, J.; Albiez, M.; Ummenhofer, T.; Sander, S.; Meschut, G.; Kötz, F. Life Prediction of Adhesive Steel Joints Under Ageing Stress – Parameter Identification and Model Verification (to be published).
[62] Bues, M.; Schuler, C.; Albiez, M.; Ummenhofer, T.; Fricke, H.; Vallée, T. Load Bearing and Failure Behaviour of Adhesively Bonded Glass-Metal Joints in Façade Structures. *J. Adhes.* 2019, *95*, 653–674. DOI: 10.1080/00218464.2019.1570158.
[63] Sander, S.; Meschut, G.; Damm, J.; Albiez, M.; Ummenhofer, T.; Kötz, F. Methodenentwicklung zur Rechnerischen Auslegung Geklebter Stahlverbindungen unter Alterungsbeanspruchung im Stahl und Anlagenbau: Permabond (Abschlussbericht Zum IGF Vorhaben Nr. 21555 N/2, FOSTA P 1496). In Heise F.-J.; Forschungsvereinigung Stahlanwendung e. V. 2024 212: Düsseldorf, Deutschland.
[64] Crank, J. *The Mathematics of Diffusion*, 2. ed. reprint ed.; Clarendon Press: Oxford, 1976.
[65] Kachanov, L. M. Rupture Time Under Creep Conditions. *Int. J. Fract.* 1999, *97*, 11–18. DOI: 10.1023/A:1018671022008.
[66] Rabotnov, Y. N. Creep Rupture. In *Applied Mechanics*, Hetényi, M. Vincenti, WG., Eds.; Springer Berlin Heidelberg: Berlin, Heidelberg, 1969; pp. 342–349. DOI: 10.1007/978-3-642-85640-2_26.
[67] Commission of the European Communities, editor. Transactions of the 5th International Conference on Structural Mechanics in Reactor Technology. Berlin, Germany 13-17 August 1979; Vol. L: Materials Modeling and Inelastic Analysis of Metal Structures, Office for Official Publications of the European Communities: Luxembourg, 1979.
[68] Johlitz, M.; Lion, A. Chemo-Thermomechanical Ageing of Elastomers Based on Multiphase Continuum Mechanics. *Continuum Mech. Thermodyn.* 2013, *25*, 605–624. DOI: 10.1007/s00161-012-0255-8.
[69] Meschut, G.; Sander, S.; Teutenberg, D.; Matzenmiller, A.; Kroll, U. Methodenentwicklung Zur Langzeitprognose Von Klebeverbindungen Bei Kombinierter Temperatur- Und Medieneinwirkung (Abschlussbericht zum IGF-Vorhaben Nr. 19517 N, FOSTA P 1243). Düsseldorf: Forschungsvereinigung Stahlanwendung e.V; 2021).
[70] Mayer, B.; Nagel, C.; Fiedler, A.; Melz, T.; Rybar, G.; Meschut, G. *Analyse Der Schwingfestigkeit Geklebter Stahlverbindungen Unter Mehrkanaliger Belastung* (Abschlussbericht zum IGF-Vorhaben Nr. 18107 N, FOSTA P 1028). Forschungsvereinigung Stahlanwendung e.V: Düsseldorf, 2017.
[71] Tschoegl, N. W. *The Phenomenological Theory of Linear Viscoelastic Behavior: An Introduction*; Springer Berlin Heidelberg: Berlin, Heidelberg, 1989. DOI: 10.1007/978-3-642-73602-5.
[72] Wiechert, E. Gesetze Der Elastischen Nachwirkung Für Constante Temperatur. *Annalen der Phys.* 1893, *286*, 546–570. DOI: 10.1002/andp.18932861110.
[73] Christensen, R. M., editor *Theory of Viscoelasticity*, 2nd ed.; Dover Publications: Mineola, N.Y, 2003.
[74] Schwarzl, F. R. *Polymermechanik*; Springer Berlin Heidelberg: Berlin, Heidelberg, 1990. DOI: 10.1007/978-3-642-61506-1.
[75] Schwarzl, F.; Staverman, A. J. Time-Temperature Dependence of Linear Viscoelastic Behavior. *J. Appl. Phys.* 1952, *23*, 838–843. DOI: 10.1063/1.1702316.
[76] Lion, A.; Matzenmiller, A.; Meschut, G.; Teutenberg, D.; Kühlmeyer, P. *Methodenentwicklung Zur Simulation Und Bewertung Fertigungs- Und Betriebsbedingter Klebschichtschädigungen Infolge Temperaturwechselbeanspruchung (Vorhaben Nr. 369 ZN, FOSTA P 878)*; Forschungsvereinigung Stahlanwendung e.V: Düsseldorf, 2015.
[77] Meschut, G.; Matzenmiller, A. *Methodenentwicklung Zur Simulation Des Thermomechanischen Verhaltens Von Klebschichten In Hybriden Fügeverbindungen*

Während Des Aushärteprozesses (Abschlussbericht zum IGF-Vorhaben Nr. 18895 N, FOSTA P 1087). Forschungsvereinigung Stahlanwendung e. V: Düsseldorf, 2018.

[78] Findley, W. N.; Davis, F. A. *Creep and Relaxation of Nonlinear Viscoelastic Materials*; Dover Publications: Newburyport, 2013.

[79] Morland, L. W.; Lee, E. H. Stress Analysis for Linear Viscoelastic Materials with Temperature Variation. *Trans. Soc. Rheology* 1960, *4*, 233–263. DOI: 10.1122/1.548856.

[80] Onogi, S.; Sasaguri, K.; Adachi, T.; Ogihara, S. Time–Humidity Superposition in Some Crystalline Polymers. *J. Polym. Sci.* 1962, *58*, 1–17. DOI: 10.1002/pol.1962.1205816601.

[81] Maksimov, R. D.; Mochalov, V. P.; Urzhumtsev Yu, S. Time - Moisture Superposition. *Polym. Mech.* 1974, *8*, 685–689. DOI: 10.1007/BF00856097.

[82] Williams, M. L.; Landel, R. F.; Ferry, J. D. The Temperature Dependence of Relaxation Mechanisms in Amorphous Polymers and Other Glass-Forming Liquids. *J. Am. Chem. Soc.* 1955, *77*, 3701–3707. DOI: 10.1021/ja01619a008.

[83] Ma, X.; Jansen, K. M. B.; Ernst, L. J. Moisture Effects on the Creep of Thermosetting IC Packaging Polymers. 7th. Int. Conf. on Thermal, Mechanical and Multiphysics Simulation and Experiments in Micro-Electronics and Micro-Systems, IEEE: Como, Italy, 2006; pp 1–5. DOI: 10.1109/ESIME.2006.1644008.

[84] Zheng, G. Influence of Moisture Content and Time on the Mechanical Behavior of Polymer Material. *Sci. China. Ser. E* 2004, *47*, 595. DOI: 10.1360/0.4ye0119.

[85] Kötz, F. Modellierung Und Numerische Simulation Der Langzeitfestigkeit Von Strukturellen Und Semistrukturellen Klebstoffen Unter Hygro-Thermo-Mechanischer Belastung.(Dissertation). Universität Kassel, to be published.

[86] DIN EN ISO 8501-1: Vorbereitung von Stahloberflächen vor dem Auftragen von Beschichtungsstoffen - Visuelle Beurteilung der Oberflächenreinheit. *Teil 1: Rostgrade Und Oberflächenvorbereitungsgrade Von Unbeschichteten Stahloberflächen Und Stahloberflächen Nach Ganzflächigem Entfernen Vorhandener Beschichtungen* 2007.

[87] Viana, G.; Costa, M.; Banea, M.; Da Silva, L. A Review on the Temperature and Moisture Degradation of Adhesive Joints Proceedings of the Institution of Mechanical Engineers, Part L: Journal of Materials: Design and Applications. 2017; Vol. 231 5, pp 488–501. DOI: 10.1177/1464420716671503.

[88] Zhou, J.; Liu, Z.; Zhu, Z.; Zeng, Z.; Sun, L. The Kinetics of the Polyurethane Moisture Curing Reaction: A Combined Experimental and DFT Mechanistic Study. *React Chem. Eng.* 2025, *10*, 38–47. DOI: 10.1039/D4RE00385C.

[89] Loh, W. K.; Crocombe, A. D.; Abdel Wahab, M. M.; Ashcroft, I. A. Environmental Degradation of the Interfacial Fracture Energy in an Adhesively Bonded Joint. *Eng. Fract. Mech.* 2002, *69*, 2113–2128. DOI: 10.1016/S0013-7944(02)00004-8.

[90] Sugiman, S.; Crocombe, A. D.; Aschroft, I. A. Experimental and Numerical Investigation of the Static Response of Environmentally Aged Adhesively Bonded Joints. *Int. J. Adhes. Adhes.* 2013, *40*, 224–237. DOI: 10.1016/j.ijadhadh.2012.08.007.

[91] Liljedahl, C. D. M.; Crocombe, A. D.; Wahab, M. A.; Ashcroft, I. A. The Effect of Residual Strains on the Progressive Damage Modelling of Environmentally Degraded Adhesive Joints. *J. Adhes. Sci. Technol.* 2005, *19*, 525–547. DOI: 10.1163/1568561054352513.

[92] Fuensanta, M.; Jofre-Reche, J. A.; Rodríguez-Llansola, F.; Costa, V.; Martín-Martínez, J. M. Structure and Adhesion Properties Before and After Hydrolytic Ageing of Polyurethane Urea Adhesives Made with Mixtures of Waterborne Polyurethane Dispersions. *Int. J. Adhes. Adhes.* 2018, *85*, 165–176. DOI: 10.1016/j.ijadhadh.2018.06.002.

[93] Ezazi, M.; Ye, Q.; Misra, A.; Tamerler, C.; Spencer, P. Autonomous-Strengthening Adhesive Provides Hydrolysis-Resistance and Enhanced Mechanical Properties in Wet Conditions. *Molecules* 2022, *27*, 5505. DOI: 10.3390/molecules27175505.